

FOR FORMER TRAN ⁷⁸⁻¹¹

2

AD A 054311

6

Nitramine Smokeless Propellant Research.

9

Annual Research Progress Report. 1 Jul 76-30 Sep 76

10

N. S. Cohen
L. D. Strand

15 VAFOSR-ISSA-77-0001

16 2308

17 AL

ID No. / DC FILE COPY

11 November 1977

12 66p.

18 AFOSR

19 TR-78-0876

Prepared for
The United States Air Force
Office of Scientific Research
Bolling Air Force Base, Washington, D.C.
Under Research Agreements

AFOSR ISSA 77-0001

by
Jet Propulsion Laboratory
California Institute of Technology
Pasadena, California
(JPL PUBLICATION 78-6)

DDC
RECEIVED
MAY 26 1978
D

14 JPL-PUB-78-6

Approved for public release; distribution unlimited.

191 150

JOB

Prepared by the Jet Propulsion Laboratory, California Institute of Technology, for the United States Air Force Office of Scientific Research by agreement with the National Aeronautics and Space Administration.

Qualified requestors may obtain additional copies from the Defense Documentation Center; all others should apply to the National Technical Information Service.

Conditions of Reproduction

Reproduction, translation, publication, use and disposal in whole or in part by or for the United States Government is permitted.

**AIR FORCE OFFICE OF SCIENTIFIC RESEARCH (AFOSR)
NOTICE OF TRANSMITTAL TO DDC**

This technical report has been reviewed and is approved for public release IAW AFR 190-12 (7b). Distribution is unlimited.

**A. D. BLOSE
Technical Information Officer**

PREFACE

The work described in this report was performed by the Control and Energy Conversion Division of the Jet Propulsion Laboratory under Contract No. NAS7-100, Task Order No. RD-65, Amendment No. 197. This investigation was supported by the Air Force Office of Scientific Research under AFOSR Support Agreement Nos. AFOSR-ISSA-77-0002 and AFOSR-ISSA-77-0001, and this report is submitted to AFOSR as the annual progress report for the period 1 July 1976 - 30 September 1977. Norman Cohen's services as Associate Investigator were funded under JPL Contract No. 954715 to Norman Cohen Professional Services of Redlands, California.

ACCESSION No.	
DTIC	White Section <input checked="" type="checkbox"/>
DDC	Buff Section <input type="checkbox"/>
UNANNOUNCED	<input type="checkbox"/>
JUSTIFICATION.....	
BY.....	
DISTRIBUTION/AVAILABILITY CODES	
Dist.	AVAIL. and/or SPECIAL
A	

D D C
RECEIVED
MAY 26 1978
RECEIVED
D

DISTRIBUTION STATEMENT A

Approved for public release;
Distribution Unlimited

ACKNOWLEDGEMENTS

This report was prepared by N.S. Cohen and L.D. Strand, who were the principal investigators for this research program. The work was conducted within the Solid Propulsion and Environmental Systems Section of JPL, under the supervision of W. Gin and Dr. G. Varsi. The authors hereby acknowledge the interest and support of Maj. T.C. Meier, Air Force project officer. Propellants tested at JPL in the course of this program were processed at the JPL Edwards Test Station, under the supervision of W.R. West. Experiments at JPL were conducted with the assistance of H. Burris and K. Chen. Burning rate data used for further steady-state model validations were furnished by B.K. Moy of the Air Force Armament Laboratory (AFATL). Data used for time-dependent model validations were furnished by C. Lenschitz of the ARRADCOM and T.L. Boggs of the Naval Weapons Center, as co-chairmen of the JANNAF Workshop on Combustion Rate Measurement. The authors wish to express their appreciation to C.F. Price of the Naval Weapons Center for many helpful discussions regarding the closed vessel burning rate experiment and the development of the computer program reported herein.

ABSTRACT

A transient ballistics and combustion model is derived to represent the closed vessel experiment that is widely used to characterize propellants. The model incorporates the nitramine combustion mechanisms which are contained within the steady-state model developed as a part of last year's (FY 1976) research. A computer program is developed to solve the time-dependent equations, and is applied to explain aspects of closed vessel behavior. It is found that the rate of pressurization in the closed vessel is insufficient at pressures of interest to augment the burning rate by time-dependent processes. In the case of nitramine propellants, however, the cratering of the burning surface associated with combustion above break-point pressures augments the effective burning rate as deduced from the closed vessel experiment. Low pressure combustion is significantly affected by the ignition process and, in the case of nitramine propellants, by the developing and changing surface structure. Thus, burning rates deduced from the closed vessel experiment may or may not agree with those measured in the equilibrium strand burner. Application of the model to closed vessel test cases shows good agreement between theory and experiment.

Series of T-burner experiments are performed to compare the combustion instability characteristics of nitramine (HMX) - containing propellants and ammonium perchlorate (AP) propellants. It is found that the inclusion of HMX consistently renders the propellant more stable. Although ash produced by more fuel-rich propellants could have provided mechanical suppression, results from clean-burning propellants permit the conclusion that HMX reduces the acoustic driving.

Additional strand burning rate data are presented which provide further confirmation of the results of the steady-state modeling effect of FY 1976.

TABLE OF CONTENTS

		PAGE
SECTION 1	OBJECTIVE	1
SECTION 2	INTRODUCTION	2
SECTION 3	TRANSIENT COMBUSTION MODEL DEVELOPMENT	4
3.1	Review of Closed Vessel Burning Rate Data	4
3.2	Application of Simplified "P-Dot" Theory	4
3.3	The Analytical Model	9
3.3.1	Conceptual Basis	9
3.3.2	Basic Equations for a Homogeneous Propellant	9
3.3.3	Equations Related to the Surface Structure of Nitramine Propellants	12
3.3.4	Computer Programming	15
3.4	Model Results	16
3.4.1	Homogeneous Propellant Test Case	16
3.4.2	Nitramine Propellant Test Case	18
SECTION 4	COMBUSTION INSTABILITY CHARACTERISTICS OF NITRAMINE PROPELLANTS	24
4.1	Background Hypothesis	24
4.2	Propellant Selection	24
4.3	Experimental Results	26
SECTION 5	EFFECT OF NITRAMINE INGREDIENTS ON STEADY-STATE BURNING RATE	31
5.1	Preface	31
5.2	Effect of HMX Particle Size in Active Binder Propellants	31
5.3	Effect of TAGN in Active Binder Propellants	34
5.4	Matching Nitramine and Active Binder	36
SECTION 6	PRESENTATIONS AND PUBLICATIONS	41
SECTION 7	CONCLUSIONS	42
SECTION 8	REFERENCES	43

APPENDIX A	NOMENCLATURE	A-1
APPENDIX B	COMPUTER PROGRAM DESCRIPTION	B-1
B-1	Subroutines	B-1
B-2	The Combustion Model Calculations	B-3
B-3	Card Input Sequence and Standard Values	B-6
B-4	Output	B-11

SECTION 1
OBJECTIVE

The objective of this research program is to study two aspects of the transient combustion properties of nitramine smokeless propellants. One is to determine the role of the nitramine ingredient in the combustion driving of acoustic instability in solid rocket motors. The second is to determine the effect of a transient pressure environment on the combustion of nitramine propellants in armament or closed vessel apparatus. The steady-state combustion characteristics of nitramine propellants have been described as a result of work performed under AFOSR Support Agreements AFOSR-ISSA-75-0005 and AFOSR-ISSA-76-0006 (Ref. 1). The present research begins to investigate unsteady-state or transient combustion characteristics.

SECTION 2

INTRODUCTION

Nitramines are of interest for gun and rocket propellant applications because they are an energetic source of smokeless combustion products (Refs. 2-4). Recent studies have been devoted to understanding and improving the steady-state combustion characteristics of nitramine propellants (Refs. 1, 5-10). Rocket motors, are, generally, principally concerned with steady-state performance. Although it is recognized that gun propellants perform in a highly transient pressure environment, there is basis for the inference that improvements in steady-state combustion will be reflected as improvements in the transient ballistics performance (Ref. 11).

Anomalous combustion behavior can be brought about by unsteady processes occurring in combustion chambers. In rocket motors, the most prevalent behavior is combustion instability. Combustion instability is of particular concern in smokeless propellants because the absence of aluminum powder deprives the system of significant stabilization (Ref. 12). Virtually no work has been done to describe the influence of nitramines on combustion instability properties. In projectiles, the extreme transient pressure environment can alter the combustion process from the steady-state as a result of time lags in the combustion response. Although this problem has been studied extensively with respect to rocket motor ignition and controlled termination (e.g., Refs. 13-17), it has not been applied to gun propellants or to the more extreme projectile environment. Burning rates derived from closed-vessel (transient pressure) testing differ from those measured at constant pressure, which raises a question about the predictability of ballistics performance (Ref. 18). Further, the transient pressure environment may (Ref. 11) or may not (Ref. 19) aggravate any steady-state combustion anomaly to impair the quality of the impetus delivered.

It is considered that understanding the transient combustion characteristics of nitramine smokeless propellants will provide additional direction for future develop-

mental efforts. The mechanistic understanding derived from the steady-state research provides an essential background, and an understanding of the transient phenomena will afford improved tailoring and predictive capabilities.

SECTION 3

TRANSIENT COMBUSTION MODEL DEVELOPMENT

3.1 REVIEW OF CLOSED VESSEL BURNING RATE DATA

A review was conducted of available data wherein direct comparisons were made between burning rates as measured in a closed vessel (transient pressure) and as measured in a strand burner (equilibrium pressure) (Refs. 20-24). Some of the closed vessel data were accompanied by the associated test pressure-time, or pressure-dp/dt (P-dot) histories. As will be discussed below, it is important to know the P-dot values for transient analysis. Some of the data were for nitramine propellants; some were for homogeneous (unfilled single-base or double-base) active binder propellants. In general, there appears to be very good agreement between the closed vessel and strand data for the homogeneous propellants. Such was the conclusion of Grollman (Ref. 23) in his study. Figures contained in Ref. (24) show a virtual identity between closed vessel and strand data. Lenschitz' data for homogeneous propellants (Ref. 20), some of which are reproduced here as Fig. 1, also show good agreement between the two methods. On the other hand, there is a significant and consistent difference between closed vessel and strand burning rates in the case of propellants containing HMX (Refs. 20-22). Examples from Ref. (20) are presented here as Fig. 2. At low pressure, the closed vessel rate tends to lag the strand rate; at high pressure, the closed vessel rate tends to lead the strand rate. As a result, the closed vessel data exhibit a more uniform and higher apparent pressure exponent.

3.2 APPLICATION OF SIMPLIFIED "P-DOT" THEORY

Where there are differences between closed vessel and strand data, such differences have been attributed to the deductive nature of the closed vessel experiment. The closed vessel experiment measures a variable pressure versus time whereas the strand experiment measures directly the distance burned versus

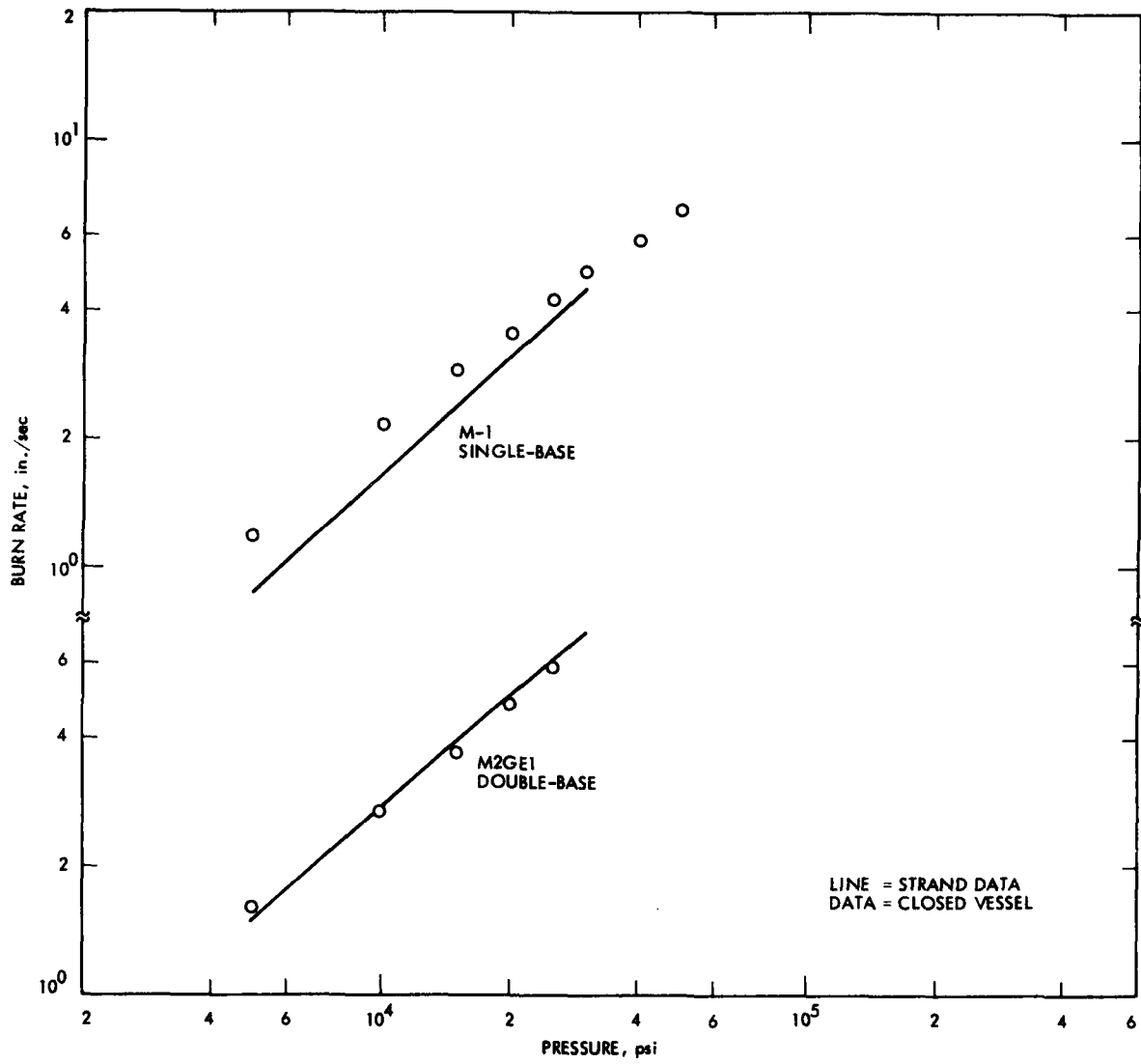


Figure 1. Comparison of Strand and Closed Vessel Data for Homogeneous Propellants

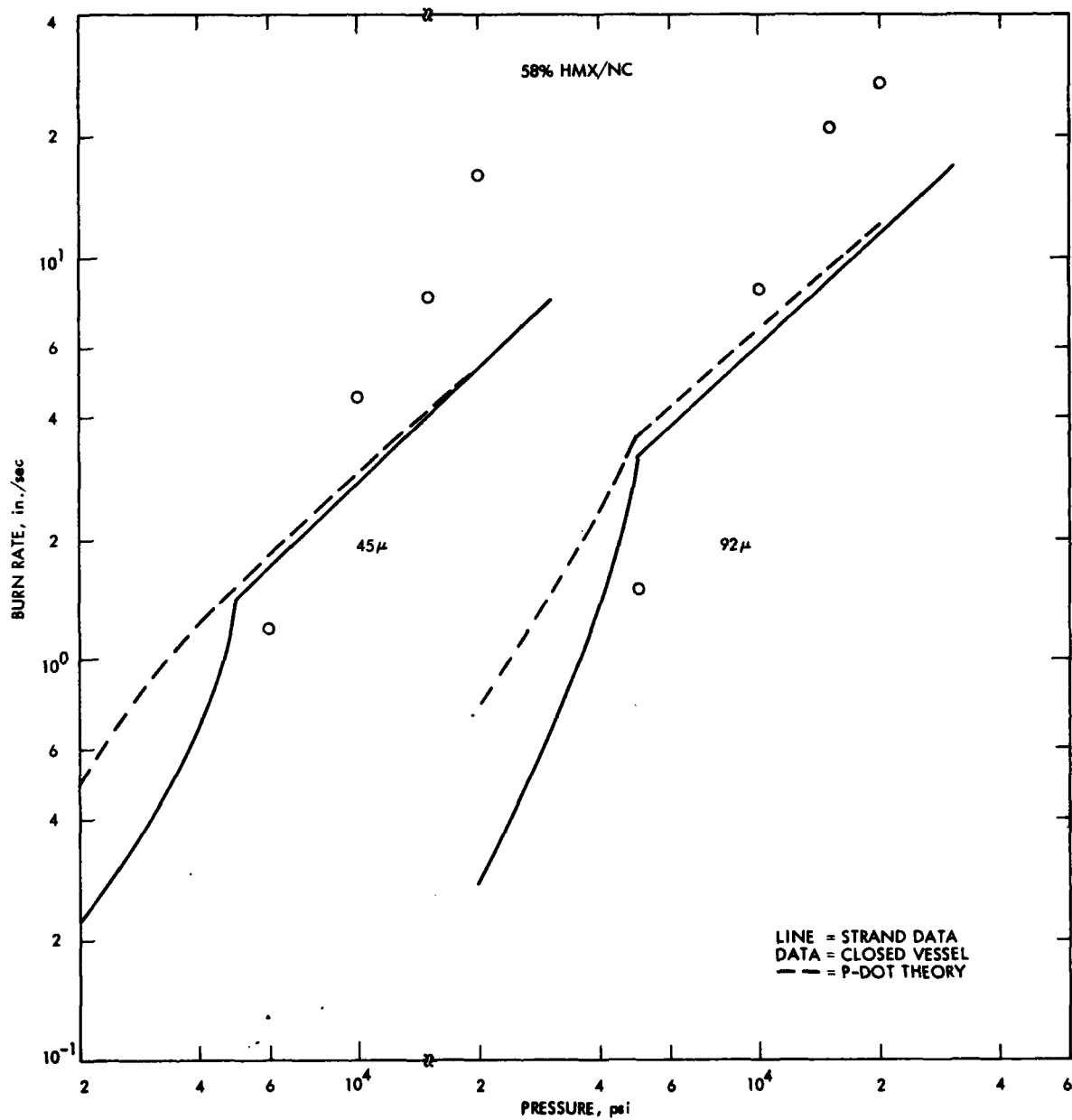


Figure 2. Comparison of Strand and Closed Vessel Data for Nitramine Propellants

time at a constant pressure. From the pressure versus time, ballistics analysis yields mass generation rate versus time if certain assumptions are made. If the geometry of the sample is known, the burning rate versus time may then be calculated. Thus, burning rate may be cross-plotted versus pressure. However, it has been suggested that the assumptions may be incorrect and that the geometry of the sample may not be known. Unknown factors frequently mentioned include heat losses, non-uniform ignition and burning, and charge break-up (Ref. 18). Low pressure uncertainties have limited the reporting of data to pressures above 5000 psi.

A mechanistic basis for a difference between burning rates measured under steady-state and transient pressure conditions was developed in the course of studies of ignition and depressurization transients in solid rocket motors (Ref. 13). This mechanism was the thermal wave relaxation time in response to a pressure transient. A simplified form of expression was as follows (Ref. 14):

$$\frac{r_i}{\bar{r}} = 1 + \frac{2n\kappa}{\bar{r}^2} \frac{\dot{P}}{P} \quad (1)$$

r_i = instantaneous burn rate at pressure, P

\bar{r} = steady-state burn rate at P

n = steady-state pressure exponent at P

κ = propellant thermal diffusivity

\dot{P} = instantaneous rate of change of pressure at P

More detailed analysis resulted in the development of computer programs such as described in Ref. (16). Some of these programs have been reviewed by Kooker (Ref. 25) in the context of gun ballistics.

An order-of-magnitude analysis of Eq. (1) reveals that P-dot effects should be small in the usual closed vessel experiment. Typical values of the parameters are as follows:

$$\bar{r} = 2 \text{ in./sec @ 10,000 psi (Fig. 1)}$$

$$n = 0.8 \text{ (Fig. 1)}$$

$$\kappa = 0.0002 \text{ in.}^2/\text{sec. (typical)}$$

$$\dot{P} = 1000 P \text{ (Ref. 20)}$$

The impact of P-dot upon burning rate falls below 10% at pressures above 10 Kpsi, and decreases with increasing pressures and burning rates. This result is consistent with the data in Fig. 1. Although the values of P-dot are very high when compared to values encountered in rocket motors, the values of pressure and r-squared also become very high so as to diminish the effect. Since most of the reported closed vessel data are at such high pressures, it would appear that agreement between the closed vessel and strand data should be expected assuming that P-dot would be the only reason for any difference. This appears to be borne out by the homogeneous propellants.

Results of P-dot calculations applied to the nitramine propellant data are included as the dashed lines in Fig. 2. It was possible to do so because the P-dot histories for these tests were available (Ref. 20). Note that the calculated effect has the tendency to reduce the pressure exponent in the high slope region below 5 Kpsi. The calculated effect becomes small at high pressure, as discussed previously. However, the data behave quite differently from the calculated effect. In view of the fact that experimental uncertainties and P-dot effects appear to be adequately resolved in the case of homogeneous propellants, it follows that something different must be happening in the case of nitramine propellants.

3.3 THE ANALYTICAL MODEL

3.3.1 Conceptual Basis

The analytical model for the transient combustion of nitramine propellants is based upon the nitramine surface structure mechanisms contained within the steady-state model (Refs. 1, 7), coupled to a thermal wave relaxation model (Ref. 16) of a homogeneous solid.

At low pressure, and following ignition, a planar melt layer must form and develop. This development will be an endothermic contribution to the energy balance, will tend to oppose the ordinary collapsing of the thermal wave during a pressure rise, and will tend to delay a break point. These effects should produce a burning rate lag at low pressure. At high pressure, and where coarse particles are present, the development of the surface craters in accordance with break points will increase the burning surface area and thereby augment the mass burning rate. As discussed earlier, the closed vessel deduces the mass burning rate and does not measure directly the linear burning rate. Therefore, if the burning surface is underestimated, the linear rate as computed from the closed vessel data will appear to lead.

Examples of cratered surfaces appear in Fig. 9 of Ref. (1). If the cratering mechanism increases both the linear burning rate and the surface area of the small pellets used in transient devices, then the mass burning rate would be proportional to the square of this process. Thus, the exponent break point would have a more serious effect in pressurizing chambers.

3.3.2 Basic Equations for a Homogeneous Propellant

Instantaneous burning rate is related to a reference or steady-state value by means of an Arrhenius equation for surface decomposition:

$$r_i = \bar{r} \exp [(-E_s/R_0)(1/T_s - 1/\bar{T}_s)] \quad (2)$$

E_s = activation energy of surface decomposition

R_0 = universal gas constant

T_s = instantaneous surface temperature

\bar{T}_s = surface temperature corresponding to \bar{r}

\bar{r} = steady-state burning rate at P, known from data or the steady-state model

The instantaneous surface temperature is calculated from the time-dependent Fourier equation:

$$\frac{\partial T}{\partial t} = \kappa \frac{\partial^2 T}{\partial x^2} - r_i \frac{\partial T}{\partial x} - \frac{AQ_{ss}}{c} \exp(-E_s/R_0T) \quad (3)$$

T = temperature distribution

t = time

x = distance into the solid

Q_{ss} = condensed phase heat of decomposition

A = prefactor

c = propellant heat capacity

For numerical solution, Eq. (3) is written in a suitable finite difference form such that the nominal mesh size is selectable depending upon the thermal wave thickness. The selection affects accuracy, stability and computer time. The initial and boundary conditions for Eq. (3), using Ref. (1) as the basis for an energy balance, are:

$$\begin{aligned}
 T(x,0) &= T_0 \\
 \frac{\partial T}{\partial x}(w,t) &= 0 \\
 \dot{Q}_s = k \frac{\partial T}{\partial x}(0,t) &= f_{\text{ext}} + \rho r_i \left\{ \left[c(T_s - T_0) + Q_{ss} \right] e^{-\xi \left[1 - (r_i/\bar{r})^2 \right]} - Q_{ss} \right\}
 \end{aligned} \tag{4}$$

w = web thickness

T_0 = initial bulk temperature

f_{ext} = external heat source, for example as would be input to produce ignition

k = propellant thermal conductivity

\dot{Q}_s = heat flux at the propellant surface

ρ = propellant density

ξ = dimensionless flame height corresponding to \bar{r} at P

The pressure variations are computed by a mass and energy balance for the chamber:

$$(V - \eta m_c) \frac{dP}{dt} = (RT_g + \eta P) \frac{dm_c}{dt} + Rm_c \frac{dT_g}{dt} - P \frac{dV}{dt} \tag{5}$$

T_g = gas temperature

m_c = mass of gas stored in chamber

R = gas constant

V = chamber gas volume

η = covolume

$$\frac{dm_c}{dt} = \rho A_b r_i \text{ and } \frac{dV}{dt} = A_b r_i \tag{6}$$

A_b = burning surface area

For a closed vessel, it is assumed that there is no mass exhaust.

$$m_c \frac{dT_g}{dt} = (\gamma T_F - T_g) \frac{dm_c}{dt} - \frac{\dot{Q}_w}{c_g} \quad (7)$$

γ = ratio of specific heats

T_F = adiabatic flame temperature (a function of P)

c_g = gas heat capacity (a function of P)

\dot{Q}_w = heat loss rate to wall

$$\dot{Q}_w/A_w = h_c(T_g - T_w) + (\epsilon\sigma)_g (T_g^4 - T_w^4) \quad (8)$$

A_w = wall area

h_c = suitable heat transfer coefficient

T_w = wall temperature

$(\epsilon\sigma)_g$ = product of gas emissivity and Stefan - Boltzmann constant

The unsteady heat transfer in the wall is solved in analogous fashion to Eqs. (3) and (4), using Eq. (8) to describe the flux at the boundary; but $r_i=0$ and $Q_{ss}=0$ for the wall.

The foregoing equations, plus Eq. (3) written for the wall, constitute a system for the unknowns P, V, m_c , T_g , \dot{Q}_w , T_w , \dot{Q}_s , T_s and r_i as functions of time. These equations are solved numerically by a forward difference method. The instantaneous burning rate will differ from the steady-state value at a given pressure to the extent that T_s differs from \bar{T}_s . This difference can arise as a result of the changing thermal profile in the solid in response to the transient heating.

3.3.3 Equations Related to the Surface Structure of Nitramine Propellants

Additional equations enter into the system for nitramine propellants because of the relationship of the surface structure to the burning rate (Refs. 1, 7) and mass flow rate. It is assumed that the surface structure will develop in three stages in the course of the pressurization transient:

- a) formation of the melt layer following ignition;
- b) disappearance of the melt layer when the break point criterion is reached;
- c) formation of the surface craters following disappearance of the melt layer.

The melt layer will start to form as soon as $T_S = T_M$, the melting point of the nitramine. The significance of the melt layer thickness is that it positions Q_{LM} , the heat of fusion, which subtracts from the exothermic Q_{SS} in the energy balance equations. It is expected that the location of T_M will move into the solid with time; T_M is 551°K for HMX, and computed steady-state surface temperatures are circa 1000°K.

The second stage commences when the critical burning rate is exceeded, $r_i > r_m$, such that subsurface melting can no longer propagate. At this time step, Q_{LM} is set to zero and the existing melt layer thickness is allowed to decompose away in accordance with the time integral of r_i in succeeding time steps. This stage is completed when the melt layer has disappeared.

The formation of the craters impacts both \bar{r} and A_b in accordance with the steady-state model. However, the development is allowed to proceed continuously with time (in the steady-state model it appears as a discontinuity with pressure). The changing surface area in the course of crater development is expressed as follows:

$$\frac{A_{bF}}{A_b} = \frac{1 - (S_{ox}/S_o)_M}{1 - (S_{ox}/S_o)_F} \quad (9)$$

A_{bF} = "frozen", or cratered surface burn area

A_b = geometric, or input burn area

$(S_{ox}/S_o)_M$ = normalized oxidizer surface exposed for a planar surface, from Ref. (7).

$(S_{ox}/S_o)_F$ = normalized oxidizer surface exposed for a cratered surface, from Ref. (7).

The parameter $(S_{ox}/S_o)_F$ changes with time because the oxidizer (nitramine) penetration depth, h , changes with time. The relationship between $(S_{ox}/S_o)_F$ and h appears in Ref. (1). The variation of the penetration depth with time may be expressed as follows:

$$dh = (r_{ox} - r_f) dt \quad (10)$$

$$r_{ox} = A_{ox} \exp(-E_{ox}/R_o T_s) \quad (11)$$

$$r_f = A_f \exp(-E_f/R_o T_s) \quad (12)$$

r_{ox} = nitramine monopropellant burning rate

r_f = binder regression rate

A_{ox} = kinetics prefactor for the nitramine

E_{ox} = activation energy for the nitramine

A_f = kinetics prefactor for binder

E_f = activation energy for binder

A limit is placed upon the extent of penetration in accordance with the steady-state model. This limit results in a maximum $(S_{ox}/S_o)_F$, or $(S_{ox}/S_o)_{MAX}$. From the steady-state model, it is known that the area change from $(S_{ox}/S_o)_M$ to $(S_{ox}/S_o)_F$ is the essential manifestation of the break point wherein \bar{r} jumps from a value influenced by the binder to a value close to the nitramine monopropellant rate. Therefore, in the course of the break point transition, it may be assumed that \bar{r} is proportional to the change in (S_{ox}/S_o) . This assumption is made in order to avoid jump discontinuities in the time-dependent model, and allow smooth (continuous) transition. Eq. (2), as applied during this third stage of surface development, becomes:

$$\frac{r_1}{\bar{r}_M} = \exp \left[(-E_S/R) (1/T_S - 1/\bar{T}_S) \right] \left\{ 1 + \left[\frac{\bar{r}_F}{\bar{r}_M} - 1 \right] \left[\frac{(S_{ox})_F - (S_{ox})_M}{(S_{ox})_F - (S_{ox})_M} \right] \right\} \quad (13)$$

\bar{r}_F = post-break steady-state burn rate

\bar{r}_M = pre-break steady-state burn rate

$(S_{ox})_F$ = that value associated with \bar{r}_F

It is anticipated that the break point in the time-dependent model need not occur at the same pressure as in steady-state. That is, the pressures for $r_i > r_m$ and $\bar{r} > r_m$ may be different. Thus it is necessary to include values of \bar{r} which extrapolate planar surface values (\bar{r}_M) to higher pressure and cratered surface values (\bar{r}_F) to lower pressure. If the cratering actually occurs at some different pressure than steady-state, a proper value of \bar{r} may still be used in accordance with the surface existing at the time.

The additional unknowns presented by nitramine propellants are $(S_{ox})_M$, r_{ox} , r_f , h , $(S_{ox})_F$ and A_{bF} . Eqs. (9-12) and two equations from the steady-state model are included in the forward difference scheme to provide the relationships. Eq. (13) substitutes for Eq. (2), and A_{bF} is used in Eq. (6). The changing surface structure is an added means by which the instantaneous burn rate may differ from the equilibrium value, and a difference between A_b and A_{bF} would bear upon effective burning rates deduced from the closed vessel experiment. The effective burning rate is obtained by multiplication of Eqs. (9) and (13).

3.3.4 Computer Programming

A computer program providing for the numerical solution of the equations was written for operation on a UNIVAC 1108 computer. The program has been successfully rendered operational and applied to test cases. An important limitation is the run time which can be encountered at very high burning rates, because a rapid transient demands a small time step for accuracy. To minimize the impact of this dependence, a scheme which automatically adjusts the time step and the solid propellant grid to the existing transient was successfully developed. The run time for a case in which the burning rate reached 20 in/sec was 15 minutes. A description of the computer program is presented in Appendix B. A source deck and listing can be furnished upon request.

3.4 MODEL RESULTS

3.4.1 Homogeneous Propellant Test Case

The homogeneous propellant test case selected for model validation is "Test Propellant A" as specified by the JANNAF Workshop on Burning Rate Measurements, Memoranda of 26 January 1977 and 5 April 1977. This case was selected because of the extensive data provided in association with the purposes of the Workshop. Burning rates were reported by six different laboratories for a given set of specifications and closed vessel pressure-time data. However, the identity of the propellant was not disclosed and strand burning rates were not given. In the absence of strand data, the reported burning rates were used as baseline equilibrium data for purposes of model application. The data were reported over the pressure range 5Kpsi-40Kpsi. An average of the results for the six laboratories was used at each pressure, and an extrapolation was performed to complete the input down to ambient pressure. Although these data are closed vessel data, the model would still be useful to show the effect of the closed vessel environment, if any. If such effect is small, as expected, the model should reproduce these data as well as the measured pressure-time curve.

The burning rate results are shown in Figure 3. The solid line represents the actual closed vessel data, except for pressures below 5Kpsi wherein it is an extrapolation. The model prediction is represented by the circles. It is observed that the prediction is very close to the line between 5Kpsi and 40Kpsi, indicating a very small effect of the transient environment. In fact, the effect of the transient environment disappears completely for this test case above 13Kpsi.

An interesting undulation appears in the predicted results between 4Kpsi and 12Kpsi. It is not certain whether this reflects a real mechanism, a tradeoff between the transient combustion zone heating and transpiration cooling during the pressure rise, or is simply a result of the forward difference numerical method. Similar undulations have appeared in computerized data reduction for closed vessel burn rate (e.g., Ref. 24).

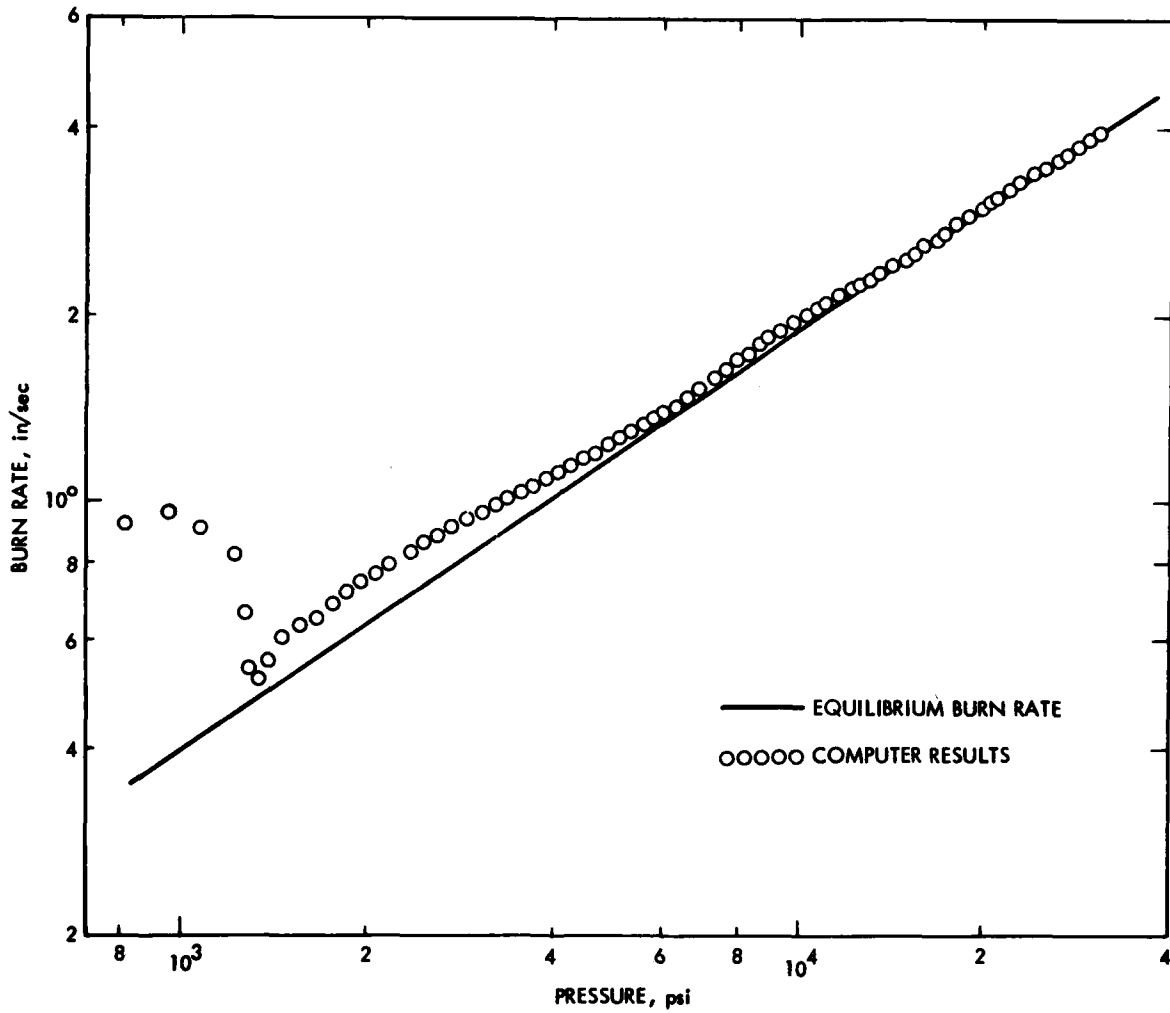


Figure 3. Predicted Effect of Closed Vessel Environment on Burn Rate of a Homogeneous Propellant

The most interesting behavior appears at low pressure. The very high initial burning rates are largely a consequence of the assumed igniter. The model does not include a representation of the igniter as such, but uses an arbitrary input heat flux to get the burning under way. If this heat flux remains operative during burning, and is large compared to the combustion-induced heat flux, the burning rate will be high. The igniter is turned off at 1000 psi, and the burning rate immediately drops because the transpiration cooling becomes excessive for the remaining heat imposed. The burning rate climbs again when the transient heating is re-established. Here, then, is a second type of burning rate undulation. A third type (not shown here) results from pre-ignition thermal soak of the propellant, or dynamic "overshoot" due to a sudden imposed compression" (25). Thus, there are mechanistic bases for low pressure burning rate undulations, depending upon the nature of the ignition process and developing combustion-induced heating. These effects, although real, are undesirable for purposes of closed vessel data acquisition and are lumped into the area of uncertainties. As a result, burning rates deduced from the closed vessel generally exclude results below 5 kpsi. An accurate quantification of the low pressure behavior would require a model of the igniter.

Predicted pressure-time results are shown together with data in Figure 4. Time is measured from ignition time rather than zero time to remove the difference in ignition delay and afford a better visual comparison. Initial pressurization is overpredicted because of the effect of the assumed igniter. This also causes the predicted web to advance relative to the actual web at a given time and pressure. The curves then merge and the prediction becomes very good at the higher pressures. The pressure results are consistent with the burning rate results.

3.4.2 Nitramine Propellant Test Case

The nitramine propellant test case selected for model validation is the 92-micron HMX propellant reported by Lenschitz (Ref. 20). Much of the required

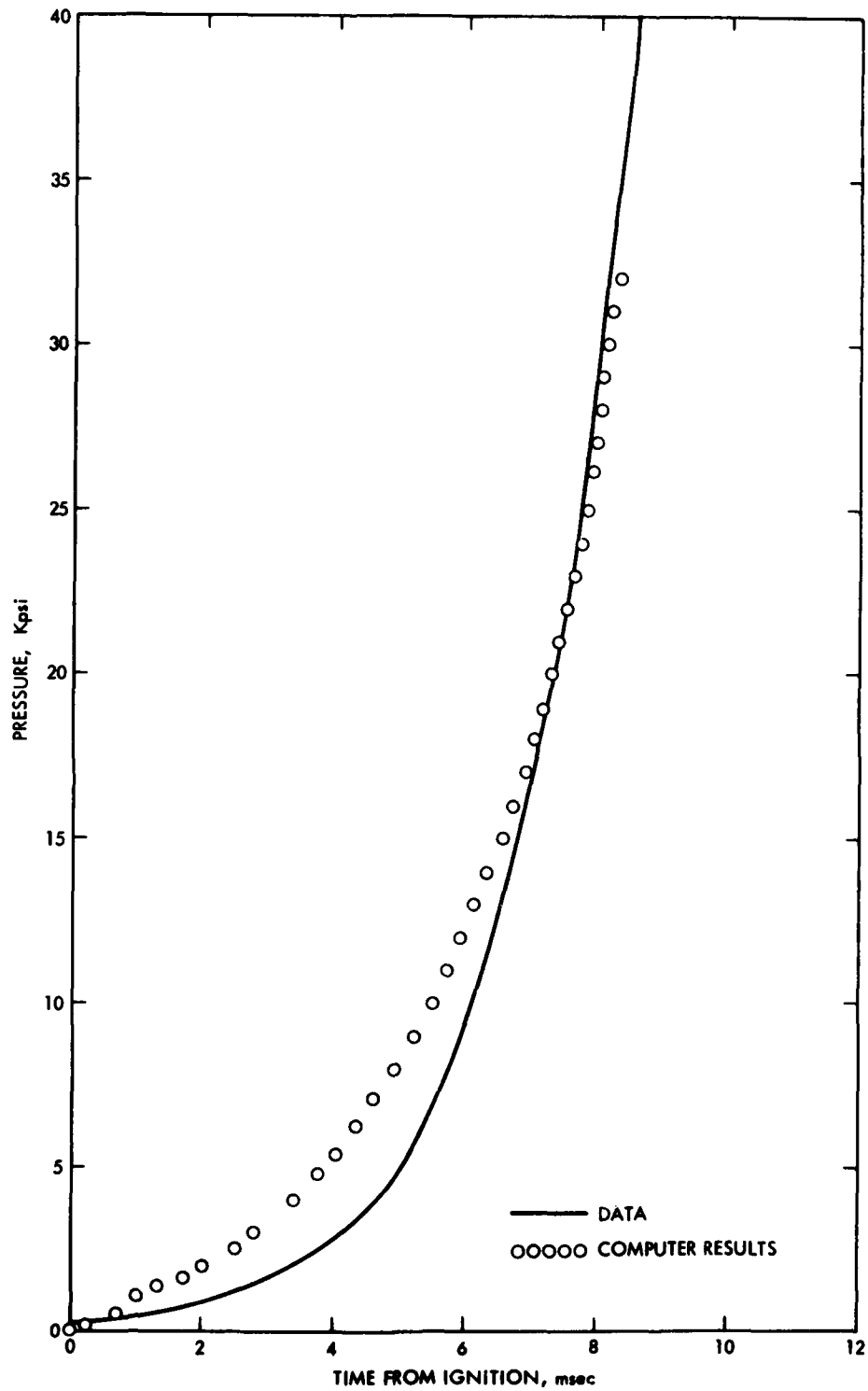


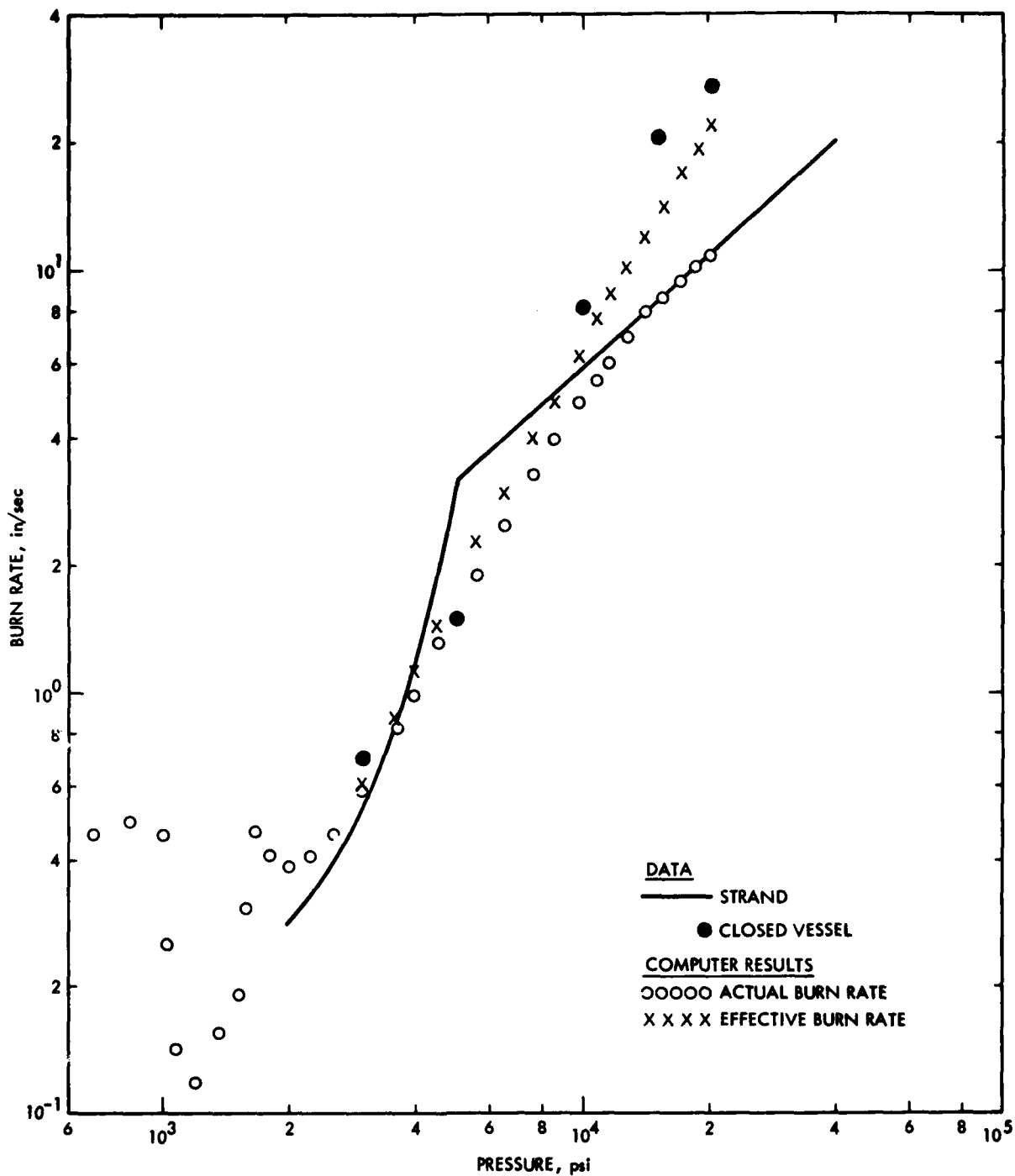
Figure 4. Comparison of Predicted and Experimental Pressurization for the Test Corresponding to Figure 3

input information is contained within that paper, including actual strand burning rate data to serve as the equilibrium baseline. The paper also reports the pressurization history for that test. Other information required was furnished by Lenschitz.

The burning rate results are shown in Figure 5. Plotted are the strand data (solid line), deduced closed vessel data (solid circles), and the predicted actual (open circles) and effective (x) burning rates in the closed vessel. As expected, there is a significant difference between strand and closed vessel burning rates in the case of a nitramine propellant, and the model serves to explain why.

First, let us examine the region below 2000 psi. Here, much the same behavior appears as was discussed for the homogeneous propellant; the burning rate is first dominated by the behavior of the assumed igniter, and drops when the igniter is turned off. Note, however, the appearance of a second burning rate undulation just below 2000 psi. This is a consequence of a fourth mechanism for undulation, and will be unique to nitramine propellants which exhibit a break point. What is happening here is that a break point is being traversed, causing a greater burning rate than can momentarily be sustained by the combustion heating then in existence. The rate falls until sufficient heating develops to re-sustain it. If the rate fell to the extent that the surface melt layer would re-form, then an endotherm would reappear to drop the rate further; such a process might appear as a fifth mechanism for undulation. No data are reported below 2000 psi, but the model results are not expected to be accurate in that regime because the igniter is not modeled.

The region between 2000 psi and 10 Kpsi is interesting because it shows how the predicted actual burning rates in the closed vessel differ from equilibrium data. Basically, the post-break-point surface structure cratering of the propellant is developing continuously and gradually in the course of the transient in the closed vessel. This continuous development lags the step-wise cratering at the



discrete test-to-test pressure intervals in the strand burner. Thus, the severity of the break point, as measured by the exponent in this transition region, is lessened by the closed vessel environment. At pressures above 10Kpsi, the predicted actual burning rates in the closed vessel merge with the equilibrium strand data as the surface structure becomes fully developed.

Comparison between predicted and measured burn rates in the closed vessel requires use of the predicted effective burn rate, because that parameter accounts for the effective propellant burn surface area due to the cratering. The predicted effective burn rate does not depart significantly from the predicted actual burn rate until pressures in excess of 3Kpsi. Over the range 3Kpsi-20Kpsi, the predictions are generally on the low side, but agree rather well with the data. Thus, it is concluded that the high closed vessel burn rates at high pressure, relative to the strand data, are due entirely to a surface area effect and not a transient burn rate effect. Lenschitz had rendered a similar conclusion (Ref. 20), but thought that the propellant grains were breaking up. Grain breakup is not required to explain these results if the cratered surface structure is recognized.

The predicted pressurization is compared with data in Figure 6. Here, the data were reported as rate of change of pressure versus pressure rather than as pressure versus time. This is a more severe test of the model because a number of factors enter into the rate of pressure change at a given pressure. The prediction falls below the data, which is consistent with the underprediction of the effective burn rates, but the agreement is rather good considering all of the factors involved.

Based upon the results of this effort and the steady-state modeling effort, it would be expected that closed vessel burning rates should agree with strand burning rates when the HMX particle size is sufficiently fine that there is no break point or surface cratering.

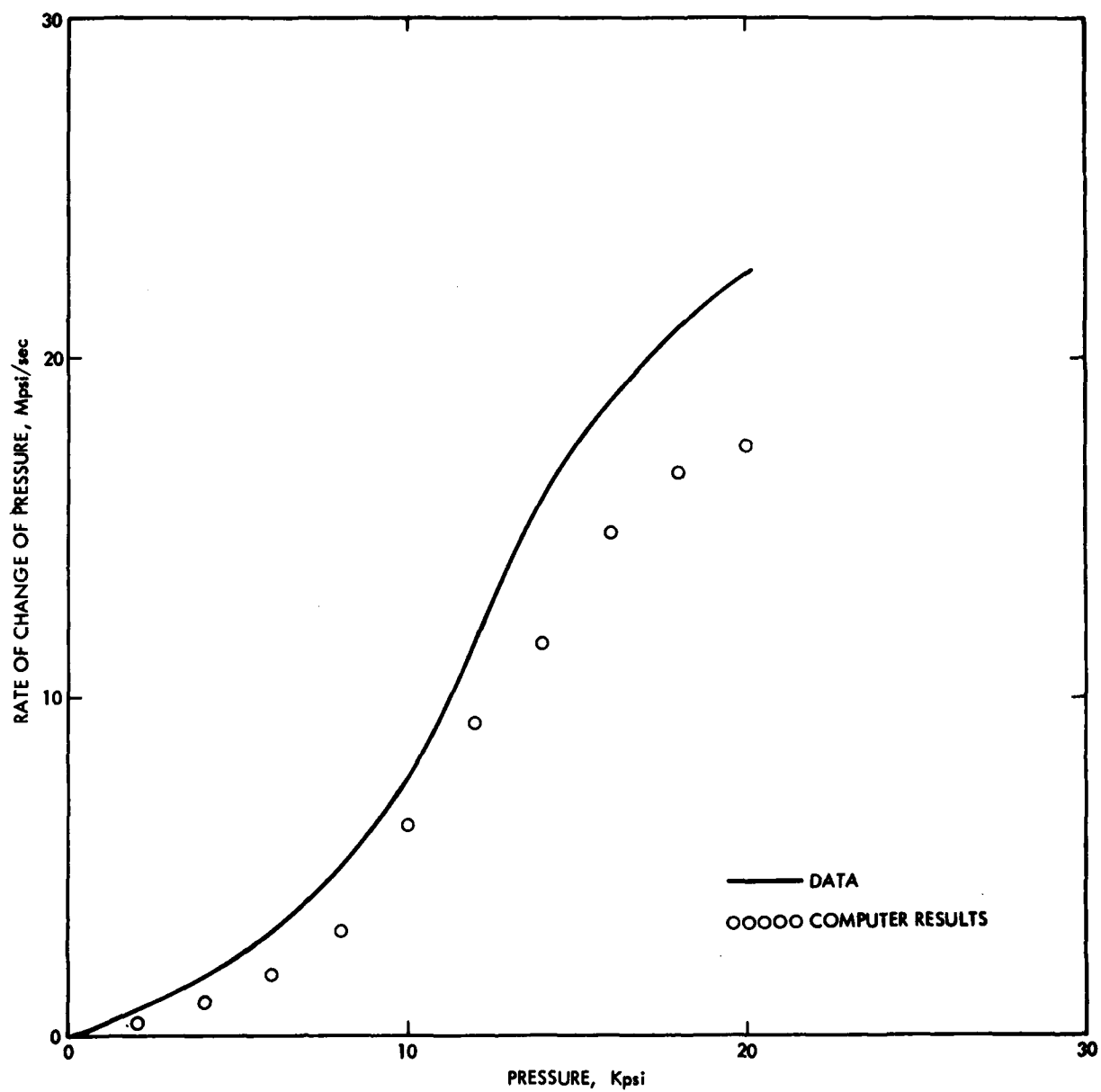


Figure 6. Comparison of Predicted and Experimental Pressurization for the Test Corresponding to Figure 5

SECTION 4

COMBUSTION INSTABILITY CHARACTERISTICS OF NITRAMINE PROPELLANTS

4.1 BACKGROUND HYPOTHESIS

A belief that HMX may have favorable effects upon combustion instability driving, relative to AP, is based upon the qualitative information presented in Table 1. With respect to some factors which may be important, HMX appears to be more similar to ammonium nitrate (AN) and potassium perchlorate (KP) than to AP. Propellants based upon AN or KP have not been reported to be unstable (Ref. 26). HMX is similar to AN and KP in that there is a substantial oxidizer melt layer and particle size effects upon burn rate are relatively weak.¹ However, HMX surpasses AP as an energetic monopropellant. To the extent that the products of combustion include particulates which may afford acoustic damping, HMX would tend to produce more carbonaceous residue than AN (but perhaps not as effective as spherical KCl droplets). At the commencement of this work, there was no reported systematic study of the effect of HMX on combustion driving.

4.2 PROPELLANT SELECTION

Standard thermochemical calculations and burning rate model calculations were performed to provide selection of the propellant formulations for T-burner combustion instability experiments. The purpose is to determine the effect of replacing ammonium perchlorate (AP) with HMX on the response function of inert binder (HTPB) propellants, and of HMX addition on the response function of nitrocellulose (NC) propellants. In making these comparisons, it was desired to maintain propellant energy and burning rate reasonably constant within each group. Although differences can be corrected in the course of interpreting the response function, it is considered that excessive differences will render the comparison less meaningful due to mechanistic bias.

¹ True at pressures below the HMX break point. Significant changes occur above the break point, which would alter the hypothesis. Pressures of interest in solid rockets, as opposed to guns, are generally below these break points.

TABLE 1

PREMISES FOR COMBUSTION STABILITY OF HMX PROPELLANTS

	<u>AP</u>	<u>AN</u>	<u>KP</u>	<u>HMX</u>
Propensity Toward Instability	Yes	No	No	?
Substantial Oxidizer Melt	No	Yes	Yes	Yes
Burn Rate as Function of Particle Size	Strong	Weak	Weak	Weak
Condensed Phase Heat Release	Strong	Weak	None	Strong
Monopropellant Flame Energy	Weak	Weak	None	Strong
Particulates in Combustion Zone	No	??	Yes	??

* - Depends on fuel-richness. For a given solids loading, an HMX propellant would be more fuel-rich than an AN propellant. Although it is possible to formulate such that no free carbon would be predicted by equilibrium thermochemistry, residues are sometimes observed.

AP and HMX produce different thermochemical effects in HTPB binder because AP is an oxidizer whereas HMX is an energetic monopropellant. HMX propellants tend to be low burning rate propellants, but significant burning rate control is available in AP propellants through particle size adjustment. Tradeoff study produced the two groups of selected HTPB propellants listed in Table 2: a low burning rate group (XA) and a high burning rate group (XB). It is difficult to match AP propellant burning rates with HMX alone, so the burning rate of formulation XA-3 is lower than desired for its group although its energy level is adequate. The two mixed oxidizer propellants are more closely related to their AP analogs in burning rate and energy.

It was found that the addition of meaningful quantities of HMX to an inert-plasticized NC binder produced considerable increases in propellant energy. Use of a relatively stable energetic plasticizer (TMETN) reduced the impact of HMX addition on propellant energy, and was considered more acceptable for research purposes than nitroglycerine. The resulting propellants comprise the third group (XC) listed in Table 2. These propellants were not tested in the course of this program because additional testing of the HTPB propellants was found to be necessary in order to acquire sufficient meaningful data.

4.3 EXPERIMENTAL RESULTS

Stability tests were carried out in 2 1/2-inch diameter (I.D.) T-burners coupled directly to a surge tank. The propellant configuration used was a 3/8-inch thick disk. Data were obtained using the growth-decay technique (Ref. 27). For each propellant, tests were conducted at nominal frequencies of 500, 900, and 1900 Hz and at pressures of 500 and 1000 Psi. Several tests were performed at each condition. Many of the tests did not produce oscillations, or the data did not conform with T-burner standards, and those tests are excluded from the results.

TABLE 2
 PROPELLANT FORMULATIONS FOR T-BURNER TESTS

	<u>XA-1</u>	<u>XA-2</u>	<u>XA-3</u>	<u>XB-4</u>	<u>XB-5</u>	<u>XC-6</u>	<u>XC-7</u>
Wt-% AP(9 μ)	-	-	-	41.25	31.25	-	-
AP(50 μ)	40.00	20.00	-	-	-	-	-
AP(90 μ)	-	-	-	41.25	31.25	-	-
AP(200 μ)	40.00	20.00	-	-	-	-	-
HMX(4 μ)	-	20.00	40.00	-	22.50	-	50.00
HMX(15 μ)	-	20.00	40.00	-	-	-	-
R-45/HTPB	20.00	20.00	20.00	17.50	15.00	-	-
NC/TMETN	-	-	-	-	-	100.00	50.00
$(T_F/M)^{1/2}$ ($^{\circ}K$) $^{1/2}$	10.34	10.30	10.32	10.70	10.77	10.49	10.86
r_{1000} (in/sec)	0.26 ¹	0.21 ¹	0.16 ¹	0.48 ¹	0.43 ¹	0.30	0.33

1 - Measured Values

The results for the low rate and high rate HTPB propellants are given in Figures 7 and 8, respectively. The results are plotted as the sum of the measured growth and decay coefficients vs. frequency. The propellants were all relatively stable in that the measured growth coefficients exceeded the decay coefficients only for the two high rate propellants at the 1900 Hz, 500 psi test condition. Such behavior may subject the absolute results to criticism, but the relative results are considered valid.

The low rate XA-1 propellant was the weaker acoustic driver of the two propellants which did not contain HMX. The low rate results from the use of coarser particle sizes. Its results appear to be relatively independent of pressure. The minimum between 500 Hz and 1800 Hz is considered real because only one test out of seven conducted at 900 Hz produced measurable acoustic driving, whereas most of the excluded data at the other frequencies stemmed from poor raw data.

The two low rate propellants containing HMX exhibited unusual results. At 500 Hz, the pressure traces showed an immediate growth of oscillations following ignition to amplitudes of about 2% of the mean and then a slow decay over the duration of the burn. At 1900 Hz, the tests exhibited no oscillations at all. At 900 Hz, the 500 psi tests were like those at 500 Hz and the 1000 psi tests were like those at 1900 Hz.

Post-test examination of the XA-3 tests showed the T-burner to be full of a layered, carbonaceous char. In the 1900 Hz tests, this char appeared to have been pulverized. For the lower HMX concentration XA-2 propellant, the char was less extensive, merely coating the wall of the T-burners rather than filling the interior. The char is presumed to be due to the fuel-rich nature of the two low rate propellants containing HMX. It was somewhat surprising because prior experience with similar propellants did not encounter char. A review of the

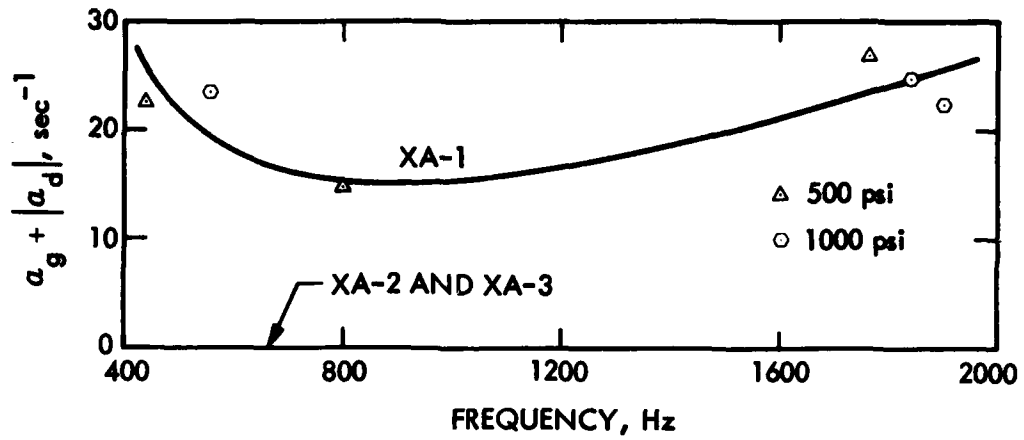


Figure 7. T-Burner Results for Low Rate HTPB Propellants

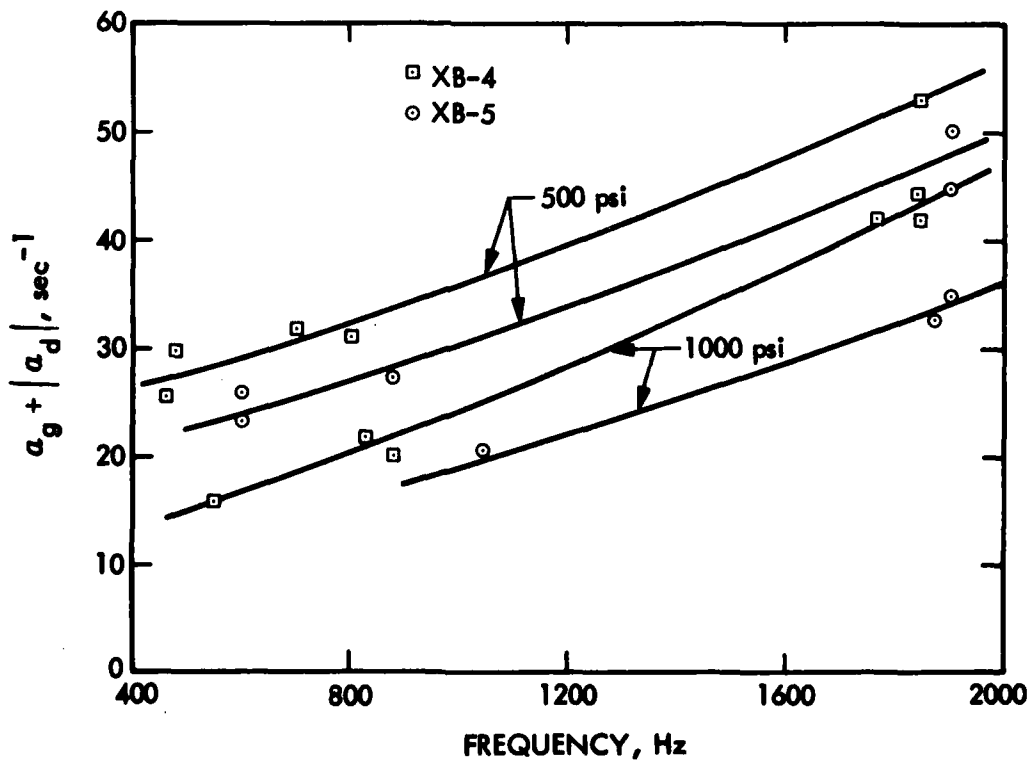


Figure 8. T-Burner Results for High Rate HTPB Propellants

formulations revealed that the prior propellants were much more heavily plasticized gun propellants, whereas the propellants formulated here were more consistent with the structural integrity requirements of rockets. Another consequence of the reduced plasticizer, or the char, was that the burning rate was about 20% lower than expected. The char is indicative of non-equilibrium thermochemistry in that there should be no free carbon at a solids loading of 80% HMX. In any event, the contribution of HMX to stability could not be identified between combustion driving or mechanical suppression from these tests.

The high rate propellant data in Fig. 8 is more conclusive as to the role of HMX. These propellants did not produce char. Both XB-4 and XB-5 showed clear pressure and frequency effects, increasing in driving strength with decreasing pressure and increasing frequency. The XB-5 HMX-containing propellant would not drive oscillations at all at the 1000 psi - 500 Hz test condition, and its data at 500 psi and 1000 psi fall below the respective data for the all-AP oxidizer XB-4 propellant. The measured damping coefficients at each frequency were about equal for the two propellants, indicating that the differences in acoustic driving are real. More data are required for clean-burning propellants, and testing of the XC group is included in future plans.

SECTION 5

EFFECT OF NITRAMINE INGREDIENTS ON STEADY-STATE BURNING RATE
(Data Supplement to Annual Progress Report AFOSR-TR-76-1136)

5.1 PREFACE

Strand burning rate data supplementing the data reported in the FY 1976 Annual Progress Report (Ref. 1) were furnished by AFATL following the publication of that Report. These data are presented and discussed in the following subsections. It is concluded that the data provide further confirmation of the results and predictions of the steady-state model developed in the course of that research.

5.2 EFFECT OF HMX PARTICLE SIZE IN ACTIVE BINDER PROPELLANTS

Figure 5 of Ref. (1) showed the effect of HMX particle size on the burning rate of nitroplasticized polyurethane (NPPU) propellant. Analogous data for NC propellant are now available and are presented in Fig. 9. The same basic trends appear as in the NPPU propellant, as was expected. The fine propellant exhibits a relatively uniform pressure exponent over two orders of magnitude of pressure. The coarse propellant begins to depart significantly at a pressure above 1Kpsi, with an upward break in pressure exponent covering the range 1.3Kpsi to 2.5Kpsi. A second upward break appears to begin at 4Kpsi and continue to high pressure. As a result, the burning rates of the coarse propellant have a multiple zig-zag appearance and are higher at high pressure. The burning rates of the NC propellants are higher than those of their NPPU analogs, which is attributed to the higher energy and burning rate of the NC binder.

A similar trend is shown by the mixed HMX-TAGN propellants in Fig. 10. A portion of the data for the propellant containing the fine HMX appeared in Fig. 7 of Ref. (1). No data were available for the propellant containing the coarse HMX. Results for both propellants are now complete. The propellant

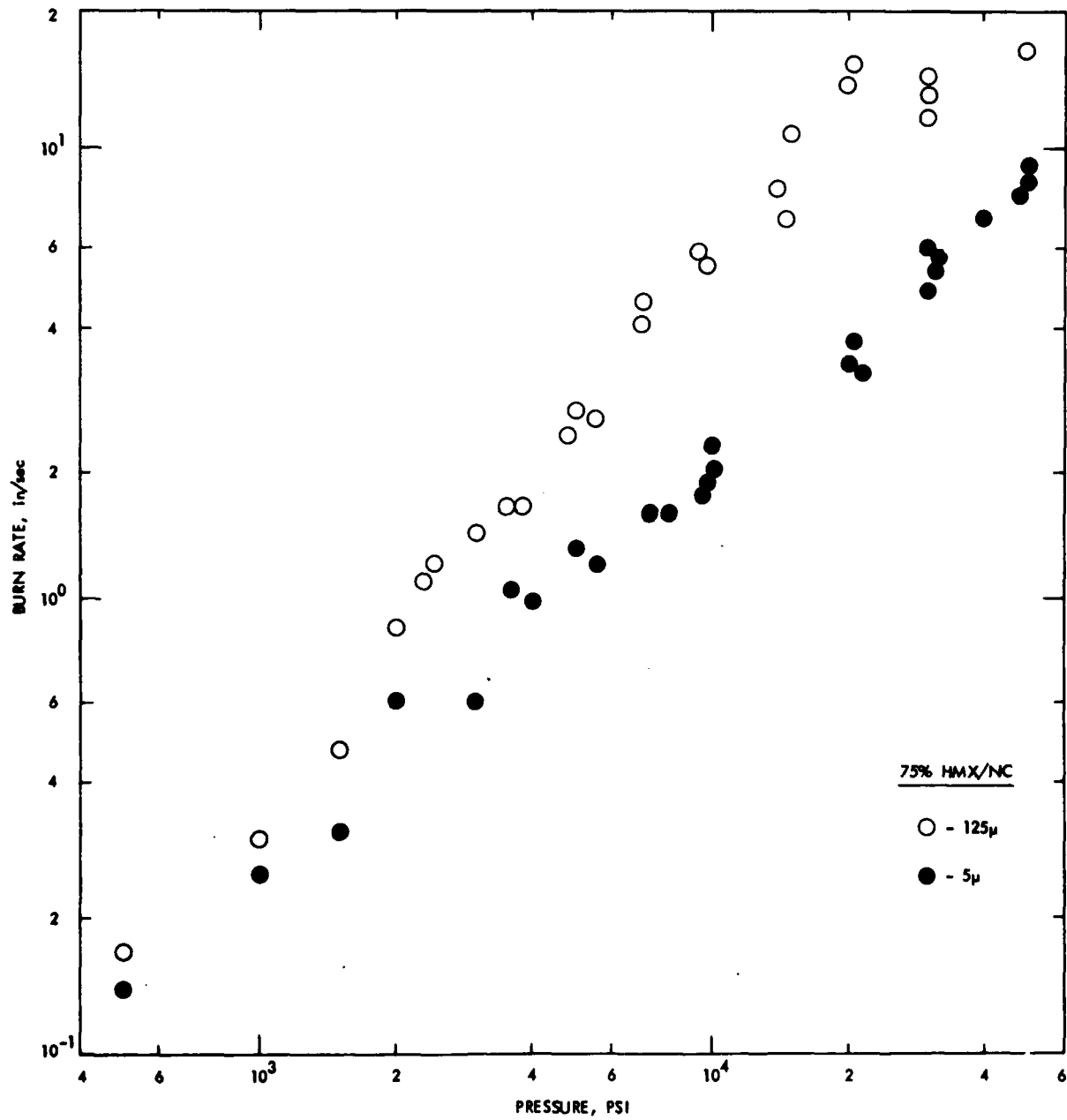


Figure 9 Effect of HMX Particle Size in Active Binder Propellants

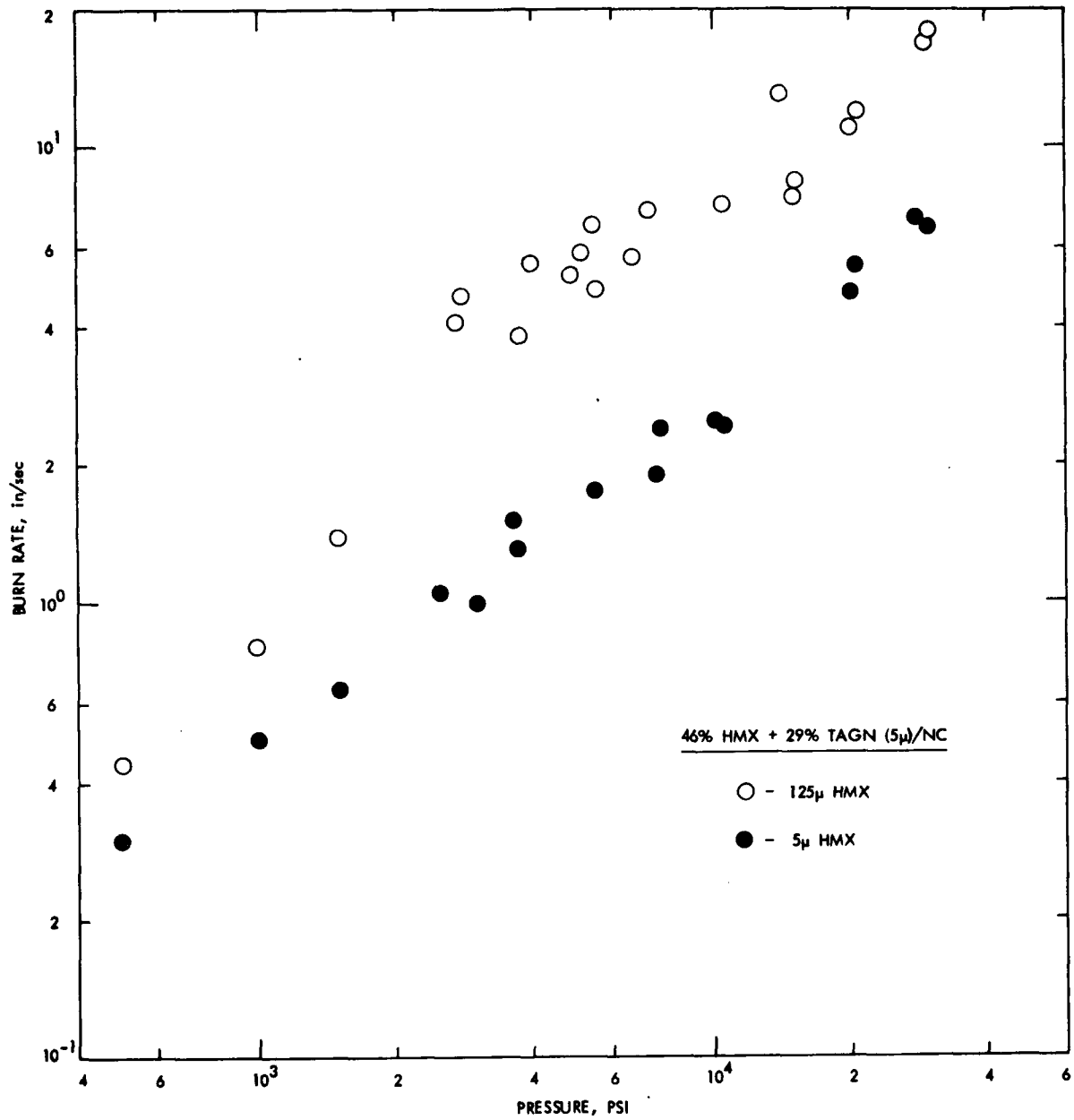


Figure 10 Effect of HMX Particle Size in Mixed HMX-TAGN, NC Propellants

containing fine HMX exhibits a relatively uniform shape over a wide pressure range. The propellant containing coarse HMX exhibits an upward break in pressure exponent covering the range 1Kpsi to 3Kpsi, such that its burning rates are higher at high pressures, as was expected. Comparing Figs. 9 and 10, the effect of the TAGN is to raise burning rates, more so at low pressure than at high pressure, such that the overall net pressure exponent is reduced. This effect has been attributed to the faster kinetics of TAGN decomposition and combustion as a monopropellant (Ref. 1).

Figs. 9 and 10 illustrate the effectiveness of fine particle size as an approach to achieve desirable slope uniformity. Fig. 9 confirms that it is possible to do so with HMX alone if the particle size is sufficiently fine. Fig. 10 confirms that TAGN addition is helpful provided that the HMX component does not exhibit a slope break.

5.3 EFFECT OF TAGN IN ACTIVE BINDER PROPELLANTS

Data presented in Figs. 9 and 10 allow the completion of Fig. 7 of Ref (1). This completed figure is presented as Fig. 11. The effect of TAGN substitution for HMX, in increasing amounts, is thereby illustrated. It was predicted that the data for the 29% TAGN propellant would interweave with the data for the 50% TAGN propellant at the higher pressures. This prediction is verified by the data. A break point appears for the 50% TAGN propellant at 10Kpsi. This was explained by the burning rates reaching such a level as to trigger the break in the HMX component, and was described as a disadvantage of excessive TAGN addition. In view of that explanation, the 29% TAGN propellant also should exhibit a break point when the burning rates reach the same level. This is not so obvious in its high pressure data, perhaps because the region is not as well characterized with data points. In any event, it is confirmed that TAGN addition raises burning rates, and that optimum amounts are helpful as an approach to achieve desired slope uniformity.

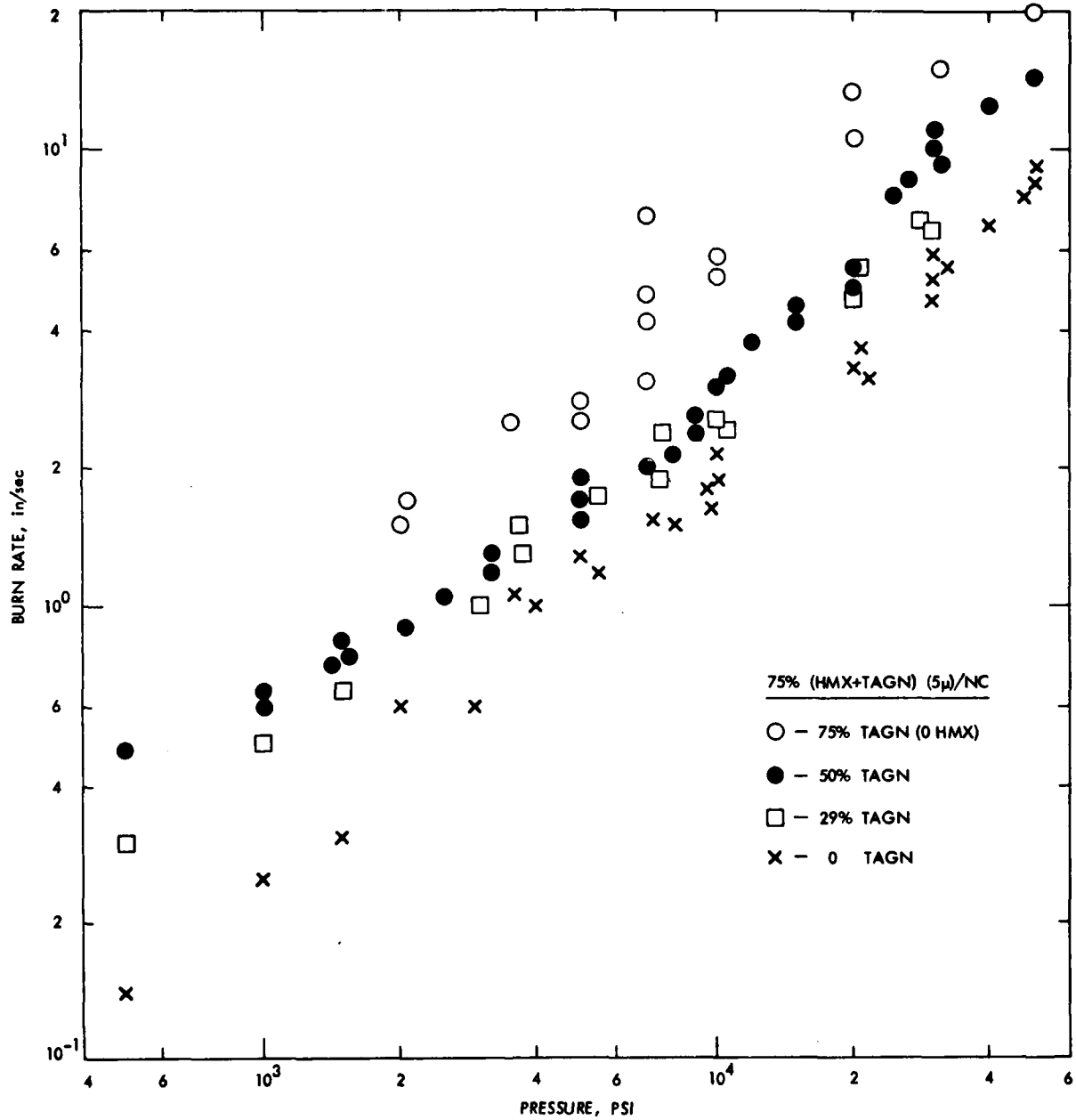


Figure 11 Effect of TAGN in NC Propellants

There has been a question as to whether or not propellants containing TAGN alone would exhibit a break point. The uppermost data in Fig. 11 are for such a TAGN propellant. The model predicted that a break point exists near the region where considerable data scatter appears, and the scatter was interpreted to be a manifestation of the break. The model also predicted that the second upward break in the 50% TAGN propellant is due to the TAGN. The question, however, could not be resolved from the data. Complete data are now available for the 63% TAGN, NPPU propellant (cf. Fig. 6 of Ref [1]). These data are shown together with the Fig. 11 data in Fig. 12. A break point for this TAGN propellant clearly appears at 10Kpsi. Therefore, it can be concluded that TAGN propellants can exhibit break points. Ironically, this break point can be mitigated by lowering the burning rates, through HMX substitution, which would yield the GAU-8 propellant. The shape of the NPPU propellant burning rate curve lends credence to the interpretation of a high slope (break) region in the case of the NC propellant. The NC propellant has higher burning rates because of the greater TAGN concentration and the more energetic binder.

5.4 MATCHING NITRAMINE AND ACTIVE BINDER

It was pointed out in Ref. (1) that matching the burning rates of the active binder and nitramine as monopropellants could yield a propellant having a uniform pressure exponent. The rationale was that a break point would have no way to manifest itself, and so would not appear in the burning rate data. In support of this hypothesis, data and results of model calculations were presented in Figs. 31-33 of that Report. These figures showed trends as the nitramine burning rate approaches and falls below the binder burning rate. It was suggested that a propellant combining fine EDNA and a tailored active binder having the same burning rates as EDNA would be a practical test of the approach.

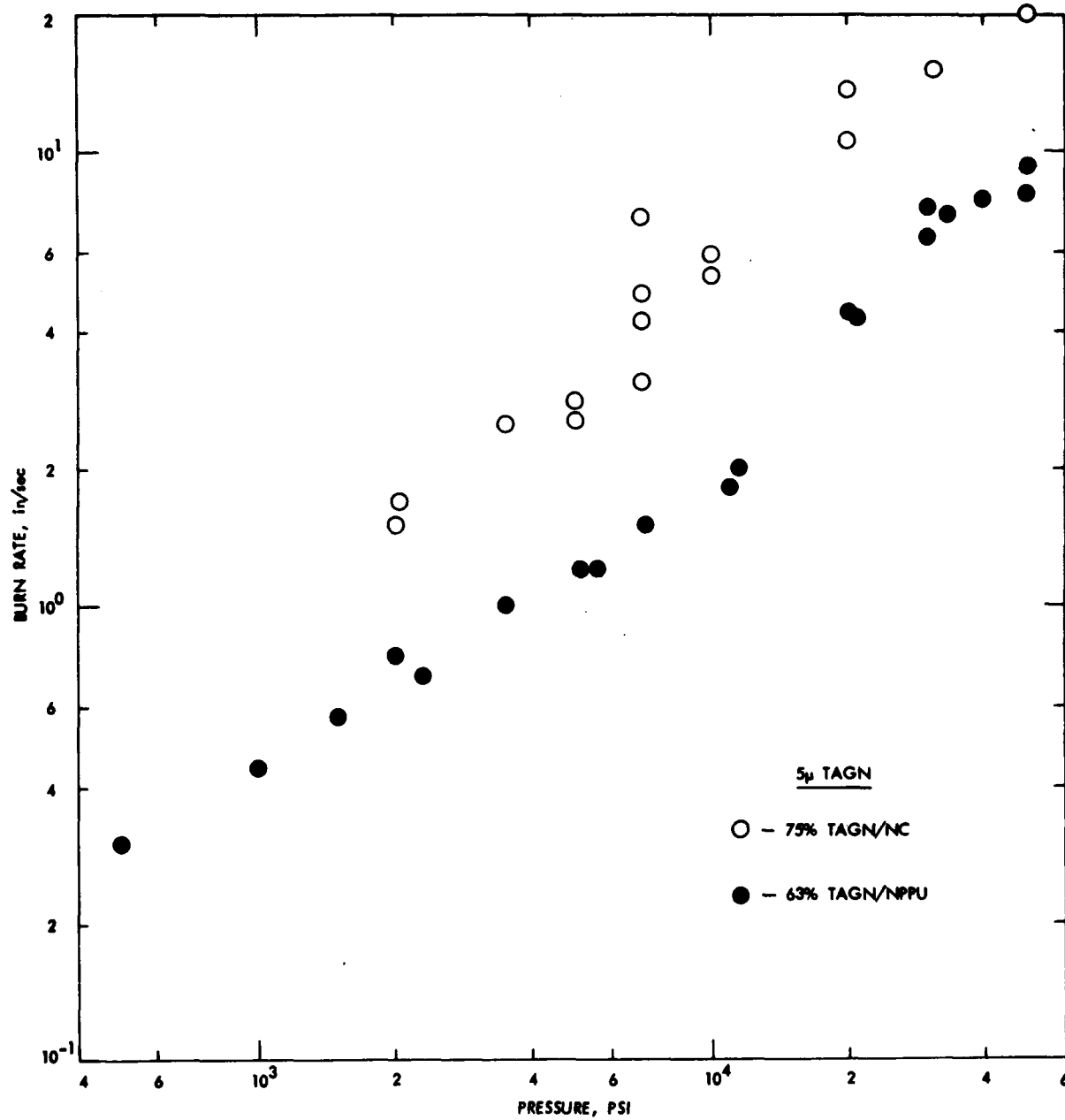


Figure 12. Burning Rates of TAGN Active Binder Propellants

Unfortunately, the propellant that was furnished combined coarse EDNA and the baseline NC binder. As a result, the binder burning rates are lower than the EDNA burning rates in accordance with the Figure 31, and the break point mechanism would be triggered at a low pressure. With this propellant, however, it is possible to complete the EDNA propellant portion of Fig. 31 and these data are shown in Fig. 13. The premise that the post-break propellant burning rates follow the nitramine monopropellant burning rates is confirmed. Without data at lower pressures, where a break would be expected, it does not appear to matter that the binder burning rates are low. A transition or jump upward to the EDNA line is not seen over this pressure range, such that this EDNA/NC propellant appears to achieve a desirable result.

An illustration of binder tailorability to implement the foregoing approach is presented in Fig. 14. The lower dashed line is for nitrocellulose (NC) containing an inert plasticizer. The upper dashed line is for nitrocellulose containing a very energetic plasticizer. The line fitting AFATL data is for nitrocellulose containing an energetic (intermediate) plasticizer. The range of burning rates is observed to cover a factor of 3. A larger range would be available by adjusting ingredient proportions, subject to energy and processing limitations; a practical range of 5 is indicated by existing active binders. The intermediate binder shown in Fig. 14 has burning rates quite close to EDNA burning rates, and would be an attractive candidate. Note, however, that the details of the binder data indicate some break point mechanism in the binder which might be reflected by the propellant using it. It is difficult to comment upon break points in active binders in general because the data are usually reported as straight lines.

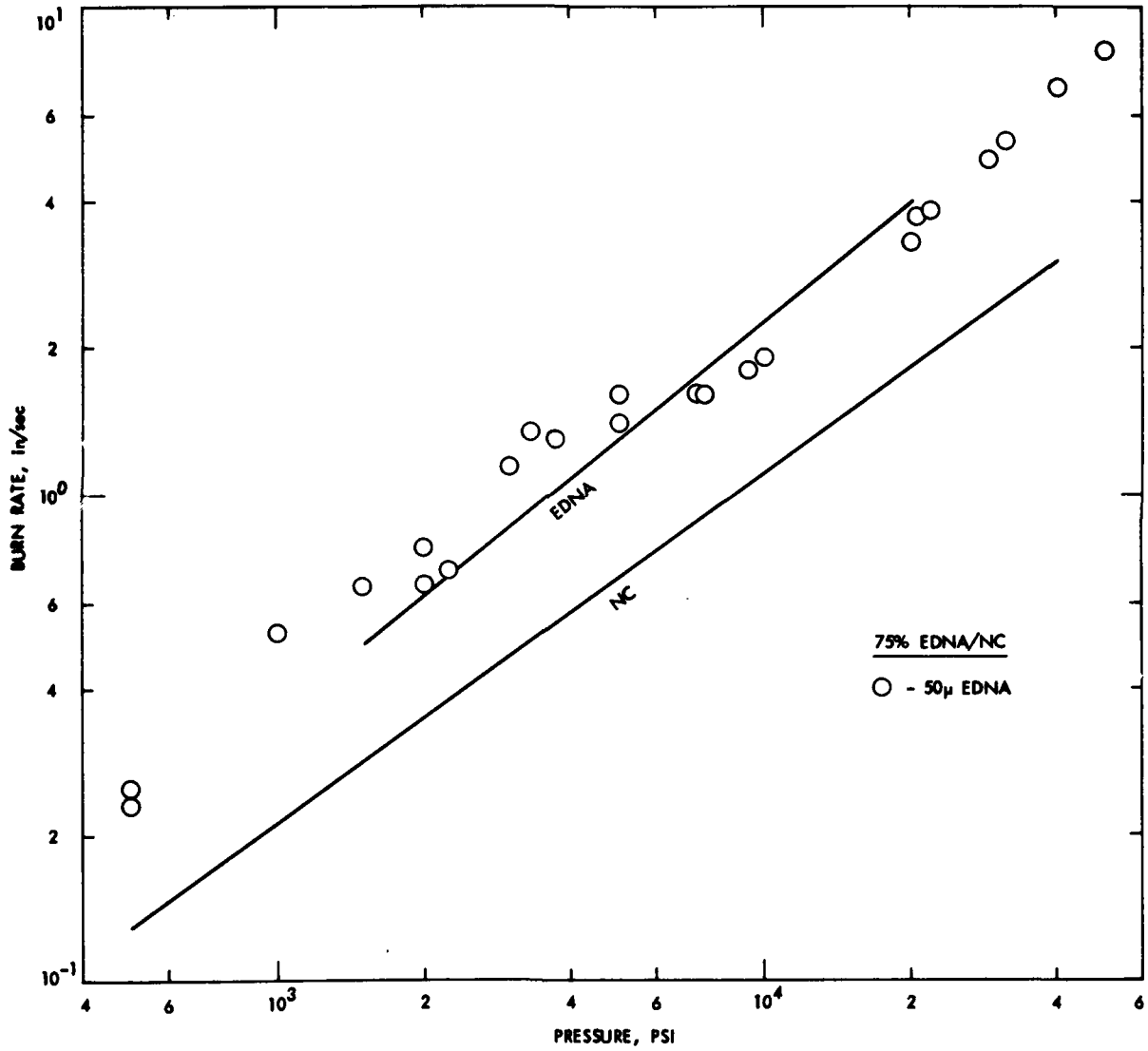


Figure 13. Comparison of Monopropellant Burning Rates and EDNA Propellant Burning Rates

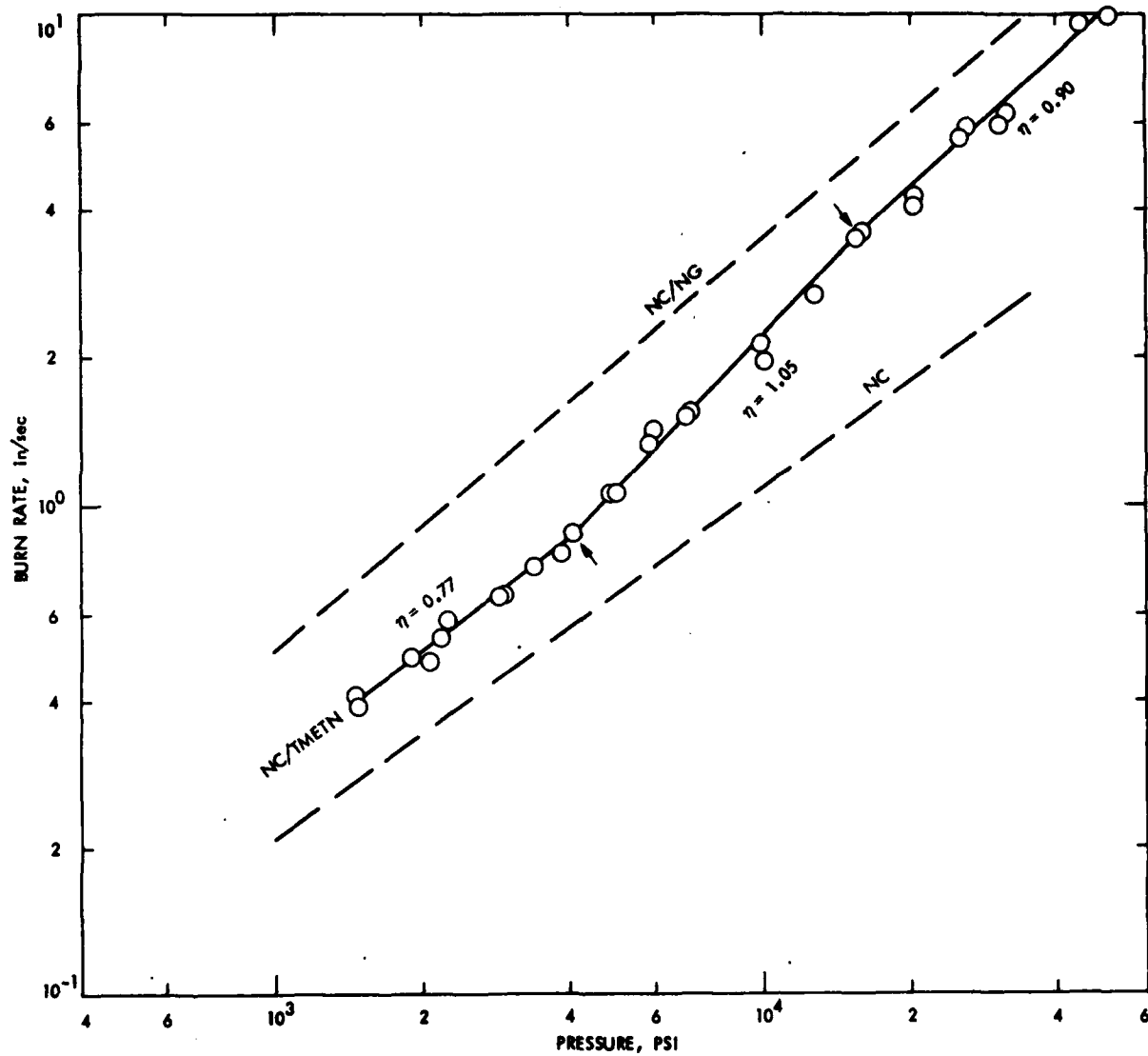


Figure 14. Effect of Plasticizer on Burning Rates of Tailored NC Binder

SECTION 6

PRESENTATIONS AND PUBLICATIONS

The following presentations and publications have been generated by this research contract:

- (1) Cohen, N.S. and Strand, L.D., "Nitramine Propellant Research", 13th JANNAF Combustion Meeting (CPIA Publication 281, Vol. I, Dec. 1976) pp. 75-87.
- (2) Cohen, N.S. and Strand, L.D., "Nitramine Smokeless Propellant Research", 1977 AFOSR/AFRPL Rocket Propulsion Research Meeting, Lancaster, CA (Mar, 1977).
- (3) Cohen, N.S., Strand, L.D., and Price, C.F., "Analytical Model of the Combustion of Multicomponent Solid Propellants", AIAA Paper 77-927, AIAA/SAE 13th Propulsion Conference, Orlando, FL (July, 1977).
- (4) Cohen, N.S. and Strand, L.D., "Transient Combustion Response Characteristics of Nitramine Smokeless Propellants", 14th JANNAF Combustion Meeting, Colorado Springs, CO (Aug., 1977), publication pending.

SECTION 7
CONCLUSIONS

A comparison of strand and closed vessel burning rate data for homogeneous propellants reveals that effects of pressurization are minor, and that the two methods should give consistent results at pressures following the ignition transient in the closed vessel. A description of burning rates during the ignition transient in a closed vessel would require a model of the igniter.

The burning rates of nitramine propellants as measured in a closed vessel will differ from strand data for those propellants which exhibit a break point. The effect of the transient environment in a closed vessel is to create a time lag in the development of the post-break-point cratered surface structure, which results in a less severe exponent shift than shown by the strand data. The reduced severity of the exponent shift will have a practical benefit in transient devices. However, the cratered surface structure will maintain high mass burning rates and exponents because of the increased burn surface area. Methods to avoid or mitigate the cratering, as discussed in the Annual Progress Report for FY 1976 (Ref. 1), are still recommended. Additional data have been presented here which confirm the conclusions of that Report.

Several mechanisms have been identified which might explain burning rate undulations often observed from closed vessel data reduction, in particular at low pressure: ignition overshoot, termination of the igniter, tradeoff between developing combustion zone-induced heating and increasing surface transpiration plus, in the case of nitramine propellants, break-point overshoot and melt layer reformation.

HMX-containing composite propellants are more stable than comparable AP propellants. One mechanism may be related to mechanical suppression due to the generation of solid material combustion products in certain fuel-rich formulations. However, it also is true that HMX reduces the combustion driving in clean-burning formulations tested thus far. Additional study is recommended.

SECTION 8

REFERENCES

1. Cohen, N.S. and Strand, L.D., "Nitramine Propellant Research", Report AFOSR-TR-76-1163, JPL TM 33-801, Jet Propulsion Laboratory, Pasadena, CA (Oct. 1976); also cf. AIAA Paper 77-927 (July, 1977).
2. Heiney, O.K., "Advanced Gun Propellants", J. Nat. Defense, Weapons Technology, pp. 152-157 (Sept. - Oct. 1973).
3. "Research Objectives Document", HQ AFSC TR 76-01 (May 1976).
4. Meier, T.C., "Air Force Rocket Combustion Research", Presentation at 13th JANNAF Combustion Meeting, Monterey, CA (Sept. 1976).
5. Steifel, L., "Review of Workshop on the Combustion of Nitramine Propellants for Guns", 10th JANNAF Combustion Meeting (CPIA Publication 243, Vol. I, Dec. 1973), pp. 199-216.
6. Kumar, R.N. and Strand, L.D., "Theoretical Combustion Modeling Study of Nitramine Propellants", J. Spacecraft and Rockets 14, 427-433 (July, 1977).
7. Cohen, N.S. and Price, C.F., "Combustion of Nitramine Propellants", J. Spacecraft and Rockets 12, 608-612 (Oct. 1975).
8. Simmons, R.L., "Workshop Report: Nitramine Gun Propellant Combustion", 13th JANNAF Combustion Meeting (CPIA Publication No. 281, Vol. I, Dec. 1976) pp. 1-8.
9. "HMX Propellant Combustion Studies", Contract F04611-75-C-0019, Hercules, Inc., Magna, UT (in progress).
10. "Improved Gun Propellant", Contract F08635-76-C-0099, Rocketdyne Division of Rockwell/International Corp., Canoga Park, CA (in progress).
11. Heiney, O.K., Presentation at the AFOSR-AFATL Explosive Combustion Meeting, Eglin AFB, FL (Apr. 1974).
12. Cohen, N.S., "Report of Workshop on Combustion Instability of Smokeless Propellants", 14th JANNAF Combustion Meeting (to be published).
13. Von Elbe, G., "Theory of Solid Propellant Ignition and Response to Pressure Transients", 19th ICRPG Solid Propulsion Conference (CPIA Publication 18, Vol. III, 1973), pp. 157-181.
14. Coates, R.L. and Cohen, N.S., "Correlation of Solid Propellant Extinguishment Data", 3rd ICRPG Combustion Conference (CPIA Publication 138, Vol. I, Feb. 1967), pp. 213-218.
15. Krier, H., T'ien, J., Sirignano, W. and Summerfield, M., "Nonsteady Burning Phenomena of Solid Propellants", J. AIAA 6, 278-285 (Feb. 1968).

16. Cohen, N.S., "Ballistic Predictions for Mass-Augmented Solid Rocket Motors", Report AFRPL-TR-71-133, Lockheed Propulsion Company (Dec. 1971).
17. Cohen, N.S. and Harry, D.P. III, "Hydroquench Thrust Termination Analysis", Report AFRPL-TR-73-62, Lockheed Propulsion Company (Aug. 1973).
18. JANNAF Workshop on Burning Rate Measurements, Calculations and Data Reduction Procedures, Ballistics Research Laboratories, Aberdeen Proving Ground, MD (Oct. 1976).
19. Rocchio, J.J., et al., "Results of Recent Experimental and Theoretical Studies of Nitramine Gun Propellant Performance", *ibid.* Ref. (8), pp. 9-19.
20. Lenschitz, C., "The Role of Thermochemistry in HMX Propellant Burning", 12th JANNAF Combustion Meeting (CPIA Publication 273, Vol. II, Dec. 1975), pp. 301-321.
21. Derr, R.L., Presentation at the AFOSR-AFATL Explosive Combustion Meeting, Eglin AFB, FL (Apr. 1974).
22. Price, C.F., private communications, Ballistics Research Laboratories, Aberdeen Proving Ground, MD (Mar. 1976).
23. Grollman, B.B. and Nelson, C.W., "Burning Rates of Standard Army Propellants in Strand Burner and Closed Vessel Tests", *ibid.* Ref. (8), pp. 21-43.
24. Mitchell, S.E. and Horst, A.W. Jr., "Comparative Burning Rate Study", *ibid.* Ref. (8), pp. 383-404.
25. Kooker, D.E. and Nelson, C.W., "Numerical Solution of Three Solid Propellant Combustion Models During a Gun Pressure Transient", 12th JANNAF Combustion Meeting (CPIA Publication 273, Vol. I, Dec. 1975), pp. 173-197.
26. Price, E.W. and Culick, F.E.C., "Combustion of Solid Rocket Propellants", AIAA Professional Study Series, p. 242.
27. "T-Burner Manual", CPIA Publication 191 (Nov. 1969).

APPENDIX A
NOMENCLATURE

A	kinetics prefactor for propellant decomposition
A_b	propellant burn surface area
A_{bF}	nitramine propellant burn surface area following cratered surface development
A_f	kinetics prefactor for binder decomposition
A_{ox}	kinetics prefactor for nitramine decomposition
A_w	surface area of closed vessel wall exposed to heating
c	propellant heat capacity
c_g	gas heat capacity
E_s	activation energy for propellant decomposition
E_f	activation energy for binder decomposition
E_{ox}	activation energy for nitramine decomposition
f_{ext}	igniter heat flux
h	depth of surface cratering in nitramine propellants
h_c	heat transfer coefficient for wall heating
k	propellant thermal conductivity
m_c	mass of gas in chamber
n	burning rate pressure exponent
P	pressure
\dot{P}	rate of change of pressure
Q_s	heat flux at propellant surface
Q_{ss}	propellant heat of decomposition
Q_w	rate of heat loss to closed vessel wall
\bar{r}	steady-state burning rate at P
\bar{r}_f	regression rate of binder
\bar{r}_F	steady-state post break point burn rate at P
\bar{r}_i	instantaneous propellant burn rate
\bar{r}_M	steady-state pre-break point burn rate at P
r_{ox}	regression rate of nitramine
R	gas constant
R_0	universal gas constant
$(S_{ox}/S_o)_M$	fraction of exposed nitramine surface on a planar melt surface
$(S_{ox}/S_o)_F$	fraction of exposed nitramine surface on a cratered surface
$(\bar{S}_{ox})_F$	value of S_{ox} associated with \bar{r}_F
t	time
T	temperature

T_F	propellant adiabatic flame temperature
T_g	instantaneous gas temperature
T_0	initial (ambient) temperature
T_s	instantaneous propellant surface temperature
\bar{T}_s	steady-state propellant surface temperature associated with \bar{r}
T_w	closed vessel wall temperature
V	instantaneous gas volume in the closed vessel
w	propellant web
x	distance from propellant surface into propellant
ϵ	radiation emissivity of gas
n	covolume
γ	ratio of specific heats
κ	propellant thermal diffusivity
ρ	propellant density
σ	Stefan-Boltzmann constant
$\bar{\xi}$	steady-state flame height associated with \bar{r} at P (dimensionless)

APPENDIX B

COMPUTER PROGRAM DESCRIPTION

B-1 SUBROUTINES

The computer program file is identified as KT, and its map of linked elements for execution is identified as KRIT. The component subroutines are listed as follows:

Segment	MAIN PROGRAM
Subroutine	EVES
Subroutine	SETUP
Subroutine	DIFEQ
Subroutine	TSWALL
Subroutine	TSPROP
Subroutine	PRINT
Subroutine	FIND

A schematic of the computer program elements is shown in Fig. B-1. Segment MAIN is the master control element. This element reads input, computes certain parameters of an input nature, writes the input, and then transfer control to EVES. Subroutine EVES is a simultaneous differential equation solver that uses the Adams predictor-corrector method. EVES sets the time step, predicts ahead, compares the results and certifies accepted answers. Subroutine SETUP initializes all of the variables, and is the first subroutine called by EVES. Thus SETUP provides the initial conditions for the time-dependent problem. Subroutine DIFEQ computes the time derivatives of gas pressure, gas volume, gas weight, gas temperature and distance burned. DIFEQ contains the time-dependent conservation equations which compute these differentials. EVES calls DIFEQ after the problem has been initialized. DIFEQ calls TSPROP to obtain the propellant combustion contributions to the conservation

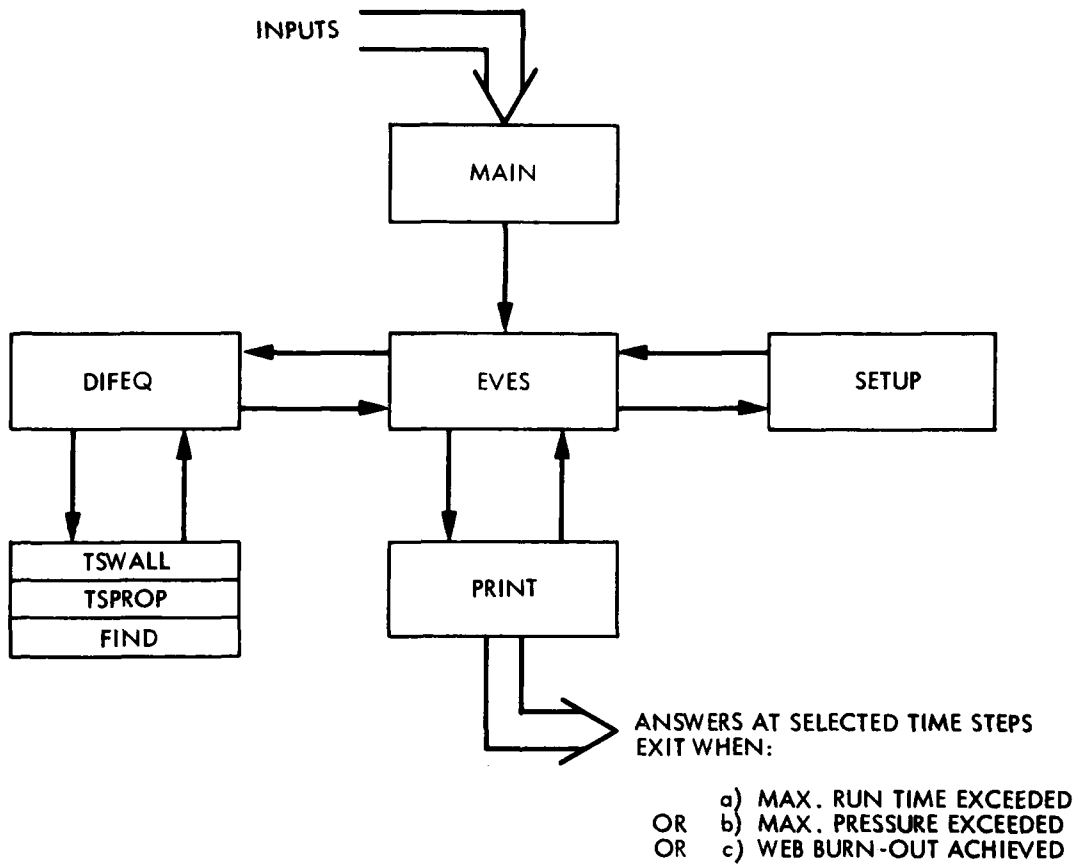


Figure B-1. Schematic of Computer Program Elements

equations, and TSWALL to obtain the heat loss to the wall which enters into those equations. TSPROP computes the time-dependent temperature profile in the solid propellant, the burning rate which is a function of surface temperature, and includes mechanisms by which nitramine behavior can influence the burning rate. A finite difference approximation of the transient heat equation is used to compute the temperature profile, which develops in response to igniter-induced heating and then to combustion heating. TSPROP may control the time step when high burn rate leads to steep temperature profiles. TSWALL computes the convective and radiation heating of the wall, and the temperature profile in the wall, in determining the heat loss. TSPROP and TSWALL return answers to DIFEQ, and DIFEQ returns answers to EVES. EVES then calls PRINT to update the accepted answers and to write them at pre-selected time intervals. Subroutine FIND is an auxiliary subroutine that is used to interpolate.

The computations involving TSPROP, which is the essence of the combustion model, warrant a more detailed discussion which is provided in Section 2 of this Appendix. A source deck and listing of the computer program can be furnished upon request; it is liberally embellished with comment cards to assist the user. A manual for inputs is provided as Section 3 of this Appendix. Output is discussed in Section 4.

B-2 THE COMBUSTION MODEL CALCULATIONS (TSPROP)

The following sequential discussion describes the computations performed in TSPROP.

1. The time step is first determined by EVES.
2. Tabular strand burning rates are initialized for the beginning of this time step.

3. The propellant web calculational mesh and counter are updated for the web which was burned away in the previous time step.
4. A further adjustment to the mesh is made depending upon whether the reference mesh is greater than $1/10$ the thermal wave thickness of the previous time step, or less than $1/25$ of that thickness. Too coarse a mesh impairs accuracy, too fine a mesh will increase computer time by requiring a smaller time step. If the mesh is adjusted, the temperature profile is redefined by logarithmic interpolation to conform to the new mesh. This technique of adjusting the mesh has provided considerable savings in computer time.
5. The time step required by the mesh is compared to the time step required by EVES, and the smaller value controls.
6. The igniter-induced heat flux is gradually diminished to zero when sufficient burning has been achieved. The method of representing the igniter is arbitrary. There is no model of the igniter as such, only an input heat flux to start.
7. The heat flux to the propellant is computed, consisting of igniter and combustion contributions. The actual heat flux is referenced from that which would exist under equilibrium burning at the pressure of the present time step, and therefore assumes a quasi-steady gas combustion zone. The appropriate tabular strand burning rate is updated to the present time step for this purpose. If the propellant is a nitramine propellant, and the actual burning rate of the previous time step is below the breakpoint burning rate, then the exothermic surface heat release term is modified by the heat of fusion of the nitramine.

8. Using a finite-difference expression, the resulting heat flux is converted into an artificial surface temperature that is used to drive the thermal profile in the depth of the solid.
9. The finite difference form of the transient heat equation is used to compute the temperature at each mesh location in the depth of the solid, including the true surface temperature. The rate of change of temperature is computed and multiplied by the time step.
10. The actual burning rate is computed from the surface temperature using an Arrhenius expression.
11. Propellant density is known from inputs. The present burn area is known from subroutine DIFEQ. Knowing the actual burn rate the propellant weight flow rate is then computed.
12. If the propellant is homogeneous, this burn rate and weight flow rate are returned to DIFEQ at this point. If the propellant is a nitramine propellant, additional computations are performed.
13. A test is made comparing the actual burning rate with the break-point burning rate. If the actual burning rate is less, the melt layer thickness of the nitramine is determined by the location of the melt temperature in the thermal profile. If the actual burning rate is now less but was at one time greater than the break point rate, such that the surface is now cratered, then an additional computation is performed to begin or continue to knit the surface back to a planar melt. This latter condition can result from depressurization or reductions in heat flux.
14. After computing the melt layer thickness, the program returns to DIFEQ if the surface is now or is once again, a planar melt. If the surface has not yet knitted completely, then adjustments are made according to the extent of cratering as discussed below.

15. If the actual burning rate is greater than the break-point burning rate in step 13, then the melt layer thickness is reduced by the product of the burning rate and the time step. If the melt layer thickness is still greater than zero, the program returns to DIFEQ. If the melt layer has disappeared by this mechanism, then the extent of cratering is computed according to the difference between the nitramine and binder burning rates. These ingredient burning rates are calculated from Arrhenius expressions for the present surface temperature. If the binder is an active binder, its rate is determined from the updated tabular input.
16. If the surface is cratered, either as a result of step 15 or step 14, the actual burning rate is upgraded in accordance with the mechanism contained in the steady-state model. The parameters which produce this upgrade are computed from the known extent of cratering and tabular burn rates as presently updated. Associated with this upgraded burn rate is an upgraded burn area, also computed from the cratering. Thus an upgraded weight flow rate is computed, and these upgraded values are returned to DIFEQ instead of the values from Step 12.

B-3 CARD INPUT SEQUENCE AND STANDARD VALUES

The following describes input cards in sequence, with appropriate comments and numerical values which have been used.

JOB CARD
SEQUENCE OF CONTROL CARDS
EXECUTION CARD

<u>CARD</u>	<u>COLUMN</u>	<u>ENTRY</u>	<u>SYMBOL</u>	<u>UNITS</u>
1	2	Type of Propellant Comment: ICASE = 1 for homogeneous propellants ICASE = 2 for nitramine propellants	ICASE	-
2	3	Title of Case or Group	ITIT	-
3	2	Initial Chamber Gas Volume	VINIT	in ³
	12	Initial Pressure	PINIT	lb/in ²
	22	Initial Temperature	TINIT	^o K
	32	Igniter Heat Flux Comment: Values of 100-200 have been used.	FEXT	cal/cm ² -sec.
	42	Reference Computational Grid size of Propellant Comment: A value of 0.0002 has been used.	DELXO	in.
	52	Computational Grid Size for Wall Comment: Divide wall thickness by 10	DELR	in.
3	62	Chamber Diameter	DIA	in.
4	2	Surface Area of Chamber Wall	AWALL	in. ²
	12	Thermal Diffusivity of Wall	ALPHAN	cm ² /sec.
	22	Flame Temperature of Propellant at 1000 psi Comment: Divide isochoric flame temperature by GAMMA	TFP	^o K
	32	Gas Molecular Weight	MW	gm/mol
	42	Ratio of specific heats	GAMMA	-
	52	Specific heat of gas at 10,000 psi	CGP	$\frac{\text{cal}}{\text{gm} \cdot \text{K}}$
	62	Specific heat of solid propellant	CSP	$\frac{\text{cal}}{\text{cal}}$
5	2	Covolume	COVOL	$\frac{\text{gm} \cdot \text{K}}{\text{in}^3}$
	12	Weight Fraction of Nitramine	ALFA	-
	22	Mean Particle Size of Nitramine	DAVE	Microns
	32	Maximum Surface Penetration Associated with Post-Break-Point Surface Cratering Comment: Use a value of 3. for sizes greater than 100 microns. Use a value of 1. for sizes less than 10 microns Use a value of 2. for intermediate sizes	HDMAX	-
	42	Nitramine density	RHOX	gm/cm ³
	52	Binder density	RHOF	gm/cm ³
	62	Propellant Thermal Diffusivity	ALPHAP	in ² /sec.

<u>CARD</u>	<u>COLUMN</u>	<u>ENTRY</u>	<u>SYMBOL</u>	<u>UNITS</u>
6	2	Reference Propellant Surface Temperature Temperature Comment: For homogeneous propellants, select a value consistent with the burning rate at 1000 psi and the kinetics expression for surface decomposition; an example is 523°K for 0.35 in/sec. and an activation energy of 50000 cal/mol. Surface temperatures for homogeneous propellants are in this vicinity. For nitramine propellants, do the same but with a pre-break-point burning rate; for example, 926°K for 0.13 in/sec and 50000 cal/mol. Nitramine surface temperatures are circa 900°K, and may be acquired from the steady-state model.	TSREF	°K
	12	Reference burning rate associated with TSREF Comment: See comment for TSREF	RREF	in/sec.
	22	Nitramine Melting Point Comment: The value for HMX is 551. The value for RDX is 467.	TMELT	°K
	32	Activation Energy for Nitramine or Homogeneous Propellant Decomposition Comment: A value of 50000. has been used for each.	ESP	cal/mol
	42	Activation Energy for Binder Decomposition Comment: Use a value of 16900. for HTPB. For active binders, input 0.	EF	cal/mol
	52	Prefactor for Nitramine Decomposition Comment: A value of 0.5000 E + 10 has been used for HMX and RDX.	ASP	$\frac{\text{gm}}{\text{cm}^2}\text{-sec}$
	62	Prefactor for binder decomposition Comment: A value of 299 has been used for HTPB. For active binders, input 0.	AF	$\frac{\text{gm}}{\text{cm}^2}\text{-sec.}$
7	2	Surface Heat Release Comment: A value of -225. has been used to represent HMX and energetic homogeneous propellants.	QSURP	cal/gm.
	12	Nitramine Heat of Fusion Comment: A value of 132.5 is used for HMX and RDX.	QLM	cal/gm
	22	Nitramine Thermal Diffusivity Comments: A value of 0.0011 has been used.	XKAPO	$\text{cm}^2/\text{sec.}$
	32	Binder Thermal Diffusivity Comment: A value of 0.0011 has been used.	XKAPF	$\text{cm}^2/\text{sec.}$
	42	Nitramine Thermal Conductivity Comment: A value of 0.00049 has been used.	XLAMO	$\frac{\text{cal}}{\text{cm-sec-}^\circ\text{K}}$

<u>CARD</u>	<u>COLUMN</u>	<u>ENTRY</u>	<u>SYMBOL</u>	<u>UNITS</u>
7 Cont'd	52	Binder Thermal Conductivity Comment: A value of 0.00044 has been used.	XLAMF	$\frac{\text{cal}}{\text{cm-sec-}^\circ\text{K}}$
	62	Wall Thermal Conductivity	XKN	$\frac{\text{cal}}{\text{cm-sec-}^\circ\text{K}}$
8	2	Number of Points in the Table of Burn Area vs Web	NWEB	-
9	2	Web Burned Comment: The first table entry should be zero	WEB1X	in.
	12	Burn area Comment: This is the total burn area at zero web burned.	ABX	in ²
REPEAT FOR NWEB CARDS TO DEFINE AREA VS WEB.				
NEXT	2	Number of Points in the Table of Pre-Break-Point Burning Rate vs. Pressure	NP1	-
NEXT	2	Pressure	PMX	lb/in. ²
	12	Pre-Break Point Strand Burn Rate Comment: Cover the full pressure range with the series of cards, extrapolating to PINIT and to the maximum pressure expected. The series may be omitted for homogeneous propellants, whence the NP1 card should be omitted also.	RMX	in/sec.
REPEAT FOR NP1 CARDS TO DEFINE PRE-BREAK-POINT BURNING RATE VS PRESSURE				
NEXT	2	Number of Points in the Table of Post-Break-Point Burning Rate vs Pressure	NP2	-
NEXT	2	Pressure	PFX	lb/in. ²
	12	Post-Break-Point Strand Burn Rate Comment: Cover the full pressure range with this series of cards, extrapolating to PINIT and to the maximum pressure expected. This series may be omitted for homogeneous propellants, whence the NP2 card should be omitted also.	RFX	in/sec
REPEAT FOR NP2 CARDS TO DEFINE POST-BREAK-POINT BURNING RATE VS PRESSURE				
NEXT	2	Number of Points in the Table of Active Binder Burning Rate vs Pressure	NP3	-

<u>CARD</u>	<u>COLUMN</u>	<u>ENTRY</u>	<u>SYMBOL</u>	<u>UNITS</u>
	2	Pressure	PBX	lb/in ²
	12	Active Binder Strand Burn Rate	RBX	in/sec.

Comment: Cover the full pressure range with this series of cards, extrapolating to PINIT and to the maximum pressure expected. This series may be omitted for inert-binder propellants, but is a must for homogeneous propellants.

REPEAT FOR NP3 CARDS TO DEFINE ACTIVE BINDER BURNING RATE VS PRESSURE

LAST CARD

B-4 OUTPUT

The initial portion of the output displays the input as groups labeled computation parameters, gas parameters, propellant parameters and the tabular input parameters. The answers are displayed in columns consisting of time, web burned, pressure, burn rate, propellant surface temperature, melt layer thickness, crater penetration depth, fraction of exposed nitramine surface area, burn area and effective burn rate. Except for burn area, the last five parameters are associated with nitramine propellants only. The effective burn rate is the actual burn rate multiplied by the ratio of the cratered surface burn area to the ideal geometric burn area, and would be the value of burn rate deduced from a closed vessel test in the absence of knowledge of the actual (cratered) burn area. The burn area which is output is the geometric (uncratered) burn area. Answers are displayed in time increments of 0.1 msec.

Computer run time may be controlled by a time stop or max time in accordance with particular facility usage, and is usually included in a control card. The run will automatically stop when the web burns out or the pressure of 40000 psi is exceeded. This maximum pressure appears in subroutine PRINT, and could be changed if desired. Full runs have ranged from 5 min.-15 min. CPU on a UNIVAC 1108.

UNCLASSIFIED

SECURITY CLASSIFICATION OF THIS PAGE (When Data Entered)

REPORT DOCUMENTATION PAGE		READ INSTRUCTIONS BEFORE COMPLETING FORM
1. REPORT NUMBER AFOSR-TR- 78 - 0876	2. GOVT ACCESSION NO.	3. RECIPIENT'S CATALOG NUMBER
4. TITLE (and Subtitle) NITRAMINE SMOKELESS PROPELLANT RESEARCH		5. TYPE OF REPORT & PERIOD COVERED INTERIM 1 Jul 76 - 30 Sep 77
7. AUTHOR(s) N S COHEN L D STRAND		6. PERFORMING ORG. REPORT NUMBER JPL Publication 78-6 8. CONTRACT OR GRANT NUMBER(s) AFOSR ISSA 77-0001
9. PERFORMING ORGANIZATION NAME AND ADDRESS JET PROPULSION LABORATORY CALIFORNIA INST OF TECH 4800 OAK GROVE DR, PASADENA, CA 91103		10. PROGRAM ELEMENT, PROJECT, TASK AREA & WORK UNIT NUMBERS 2308A1 61102F
11. CONTROLLING OFFICE NAME AND ADDRESS AIR FORCE OFFICE OF SCIENTIFIC RESEARCH/NA BLDG 410 BOLLING AIR FORCE BASE, D C 20332		12. REPORT DATE Nqv 77
14. MONITORING AGENCY NAME & ADDRESS (if different from Controlling Office)		13. NUMBER OF PAGES 62
		15. SECURITY CLASS. (of this report) UNCLASSIFIED
		15a. DECLASSIFICATION/DOWNGRADING SCHEDULE
16. DISTRIBUTION STATEMENT (of this Report) Approved for public release; distribution unlimited.		
17. DISTRIBUTION STATEMENT (of the abstract entered in Block 20, if different from Report)		
18. SUPPLEMENTARY NOTES		
19. KEY WORDS (Continue on reverse side if necessary and identify by block number) NITRAMINE PROPELLANTS TRANSIENT COMBUSTION CLOSED VESSEL AND T-BURNER		
20. ABSTRACT (Continue on reverse side if necessary and identify by block number) A transient ballistics and combustion model is derived to represent the closed vessel experiment that is widely used to characterize propellants. The model incorporates the nitramine combustion mechanisms which are contained within the steady-state model developed as a part of last year's (FY 1976) research. A computer program is developed to solve the time-dependent equations, and is applied to explain aspects of closed vessel behavior. It is found that the rate of pressurization in the closed vessel is insufficient at pressures of interest to augment the burning rate by time-dependent processes. In the case of nitramine propellants, however, the cratering of the burning surface associated		

DD FORM 1473

1 JAN 73

EDITION OF 1 NOV 65 IS OBSOLETE

UNCLASSIFIED

SECURITY CLASSIFICATION OF THIS PAGE (When Data Entered)

UNCLASSIFIED

SECURITY CLASSIFICATION OF THIS PAGE(When Data Entered)

with combustion above break-point pressures augments the effective burning rate as deduced from the closed vessel experiment. Low pressure combustion is significantly affected by the ignition process and, in the case of nitramine propellants, by the developing and changing surface structure. Thus, burning rates deduced from the closed vessel experiment may or may not agree with those measured in the equilibrium strand burner. Application of the model to closed vessel test cases shows good agreement between theory and experiment. Series of T-burner experiments are performed to compare the combustion instability characteristics of nitramine (HMX)-containing propellants and ammonium perchlorate (AP)propellants. It is found that the inclusion of HMX consistently renders the propellant more stable. Although ash produced by more fuel-rich propellants could have provided mechanical suppression, results from clean-burning propellants permit the conclusion that HMX reduces the acoustic driving. Additional strand burning rate data are presented which provide further confirmation of the results of the steady-state modeling effect of FY 1976.